Sand Dune Vegetation Monitoring and Assessment using UAV Remote Sensing: A Case Study for Karekare Beach, Auckland Region, New Zealand

Joshua Bilkey

A thesis submitted to Auckland University of Technology in partial fulfilment of the requirements for the degree of Masters of Geographical Information Science (MGIS)

School of Science

Auckland University of Technology (AUT)

2022

Supervisor/s: Dr Bradley Case, Dr Hannah Buckley & Graham Hinchliffe

Attestation of Authorship

I hereby declare that this submission is my own work and that, to the best of my knowledge and belief, it contains no material previously published or written by another person (except where explicitly defined in the acknowledgements), nor material which to a substantial extent has been submitted for the award of any other degree or diploma of a university or other institute of higher learning.

Signed:

Date: 14/02/2022

Acknowledgements

I would like to thank my supervisors, Dr Bradley Case, Hannah Buckley and Graham Hinchliffe. In particular, I would like to thank my principal supervisor Dr Bradley Case for giving me the extra push I required to complete the thesis.

I want to thank the Department of Conservation for allowing me to pursue this research within the sand dune ecology discipline.

I would also like to thank Susan Crowder, Beibei Chiou, Bonnie Brannigan and Nigel Harris for being accommodating and letting me complete the thesis after re-joining the Master's Programme.

I would also like to thank my parents, Mary and Glyn and my sister Kate for their continued support. Finally, to Leydy Johana Zambrano Cortes for always being there and giving me the support I required.

Abstract

There has been a rapid amount of ecosystem and biodiversity loss globally. Coastal ecosystems such as sand dunes have been particularly at risk, from climate change, residential intensification and invasive species (Haddad et al., 2015). This study aimed to analyse the effectiveness of Unmanned Aerial Vehicles (UAVs) for vegetation classification and monitoring.

Two main techniques were employed for vegetation classification: traditional pixel-based and Object Orientated Image Analysis (OBIA). In recent years classification algorithms have increasing focused on OBIA because of its ability to include information not solely spectral but also shape, texture, compactness and spatial relationships (Blaschke., 2013). In this study OBIA had overall accuracies of 80.09% in the March 2019 flight compared to the next best pixel-based algorithm of 75.77% for the same March Flight. The accuracies for all classification algorithms were reduced in the November 2018 Flight, 77.61% for the OBIA algorithm. This trend of lower accuracy in November was seen in the other pixel-based classification algorithms also.

While the overall accuracy was high, there were still many individual thematic classes in the study which were consistently misclassified. However, a promising result was Pampas grass/ *Cortaderia selloana* (an invasive species) achieved higher levels of accuracy when using OBIA classifications compared to pixel-based.

UAVs represent a unique opportunity for ecological research. They are relatively inexpensive, can be launched rapidly and can access areas either to remote, dangerous and reduces the environmental impacts caused by trampling via traditional field methods. As the sensor technology, UAV platform technology and classification algorithms continue to evolve, the potential for the use of UAVs in environmental research is highly promising.

Contents

List of Figures

List of Tables

1. Introduction

1.1 Sand Dunes Importance in New Zealand

Habitat and biodiversity loss are occurring rapidly within many global ecosystems. Increased public awareness has led to pressure on governing bodies to review current management processes and funding allocation for conservation measures (Haddad et al., 2015; Perring., 2012). Climate change, urban intensification and invasive plant species are critical threats to current ecosystem health. Coastal areas are particularly at risk of changing sea levels, climate change and residential intensification (Thomas et al., 2018). Sand dune vegetation is also vulnerable to invasive species due to the low levels of competition within these ecosystems (Brown and McLaughlin, 2002; Defeo et al., 2009).

Invasive species can dramatically influence the ecological function and diversity of many ecosystems globally. For example, in many coastal environments, non-native grasses on foredunes out-compete native plants and drastically alter the form and function of the dune ecosystem (Hilton, 2006; Barrows et al., 2009). The efficient sand-binding grasses, such as marram grass, were often planted for dune stabilisation to protect land with high economic value for uses such as farming, forestry or residential housing (French et al., 2011).

Dune vegetation has changed dramatically during the colonisation period of the late 1800s to early 1900 (Hilton et al., 2006). Marram grass (Ammophila Arenaria) was introduced as a dune stabiliser throughout New Zealand (Sykes and Wilson, 1991). Many studies have shown that Ammophila dominated foredunes produce large steep foredunes. Hilton and Harvey's (2002) study suggested that Ammophila dominated foredunes reduce or prevent blowouts and transgressive dune development. Transgressive dunes systems are more ecologically and morphologically diverse.

While the influence of marram grass on dune ecosystems has been studied extensively (Thomas et al., 2018), other non-native species also dominate the New Zealand coastal landscape. One of these species is tree lupin (Lupinus arboreus). Lupinus arboreus was planted in many coastal back dunes to support forestry due to its properties for nitrogen fixation (Thomas et al., 2018). Exploring the relationship between native and non-native species within the dune ecosystem and the key drivers of the distribution and abundance is essential for monitoring and restoring dune ecosystems.

Coastal dune lands are prominent around much of New Zealand's coastland. Cockayne described them as New Zealand's "most common landform" (Cockayne in Hilton et al., 2000). However, natural coastal ecosystems have been significantly reduced from pre-colonisation times (Partridge, 1992). These areas are considered of high ecological importance due to the amount of endemic vegetation within this ecosystem. In particular, species such as pingao and spinifex dominate the active foredunes and act as sand binders. The ecosystem is aeolian dominated, and the movement of sand by wind and waves and these forces dictate the morphological and ecological structure within these areas.

In New Zealand, government strategies such as the New Zealand Biodiversity Strategy (DOC and MfE) have been introduced to address the need to assess and monitor New Zealand's ecosystems. Decision making and management plans require detailed and robust information on species and habitat diversity, distribution and how these differ over time. As a result, there have been various morphological and ecological surveys of sand dunes within New Zealand. A history of the different coastal surveys is explored in the following section.

1.2 New Zealand Sand Dunes - A history of National Surveys and Classification Schemes

1.2.1 The First National Coastal Sand Dune Survey

Leonard Cockayne conducted the first coastal sand dunes survey in 1911 (Cockane, 1911). This survey aimed to assess the botany and character of New Zealand sand dunes. Dune plant associations identified in this survey included native sand binders (pingao and spinifex), grass-dominated dunes, shrub or forest cover and inter-dune wetlands and lakes (Hilton et al., 2000). He also estimated the total dune area of New Zealand to be 128,740ha (118900 in the North Island and 9840 in the South Island). In 1958, another estimation of active duneland was carried out with an estimated area of 127 000 ha being derived (Hilton et al., 2000). The 1911 survey was commissioned after the Sand Drift Act 1907 had been enacted, and, therefore, he concluded "the final treatment of dunes should assuredly be afforestation'(Cockayne 1911, p. 4). Following this report, marram grass was widely planted to stabilise the active sand dunes. Marram grass has subsequently propagated widely and is now the most prevalent invasive species in the foredune environment (Hilton et a., 2005).

1.2.2 Creation of National Inventories for Conservation Management of Coastal Environments (1990s)

The Sand Dune and Beach Vegetation Inventory was created in 1992 by the Department of Scientific and Industrial Research and represented the first national conservation assessment of New Zealand's sand dunes (Hilton et al., 2000). This assessment aimed to assess each dune system's natural and botanical values, whereby a ranking between 0 and 20 was assigned based on vegetation community and landform diversity, the proportion of native species, amount of human modification, and the proportion of invasive weed species. From the survey, a total of 53 sites were identified as nationally significant for conservation. The Inventory categorises dune vegetation zones as strandline, foredune, back dune, moist inter-

dune depressions and stone pavements (Hilton et al., 2000). The ranking assigned to each dune system is based on the ecological and morphological characteristics of these categories. However, the Inventory was criticised by Rapson (1996) for not including interdune wetland and lake habitats in addition to missing certain types of dunes. Another criticism of the Inventory was the lack of priority associated with stabilised duneland ecological characteristics (Hilton et al., 2000).

The Protected Natural Areas Program (PNAP) was created for identifying indigenous plant communities' characteristics and locations not represented by existing surveys. Recommended Areas for Protection (RAPS) are defined by the "representativeness, diversity, special features, naturalness, viability, size and shape and buffering from external stresses" (Hilton et al., 2000). A total of 179 ecological districts (EDs); however, only 25 of the 123 coastal EDs were surveyed as of 1998 (Hilton et al., 2000). The PNAP surveys identify larger ecological districts than the Sand Dune and Vegetation Inventory; therefore, back dune and stabilised indigenous forested areas at the margins of the dune area are given greater weight in the survey. However, any advantage of this methodology is offset by the lack of surveys conducted compared to the Nationwide surveys completed between 1984 and 1988 by the Sand Dune and Beach Vegetation Inventory.

The Inventory of New Zealand Active Dunelands was commissioned by the Department of Conservation and created by Hilton, Macauley and Henderson (Hilton etl al., 2000). Active dunelands from the 1950s to the 1980s were constructed from topographic maps and other ancillary information, while maps of the 1990s active duneland were created from contemporary aerial photography. It was found that active duneland had decreased from Cockayne's estimate of 129 000 ha to 39 000 ha, a 70% reduction (Hilton et al., 2000).

1.2.3 National Ecosystem Classification (2014)

The National Ecosystem Classification was created by the Department of Conservation to categorise the natural environment into defined ecosystems (Singers and Rogers, 2014). The ecosystem classification aims to describe both biotic and abiotic relationships to include "physical variable, process variables and biota" to analyse each ecosystem's environmental and physical drivers (Singers and Rogers, 2014). In this Classification, ecosystems are divided into zonal and azonal ecosystems. Zonal ecosystems drivers include macroclimatic variables such as temperature and rainfall, and azonal ecosystems are driven by edaphic extremes such as soil chemistry or extreme heat. A total of 152 ecosystems were classified, 78 zonal and 72 azonal.

In this Classification, five active coastal dunes ecosystems were identified (DN1-5), all of which are azonal ecosystems. Active dunes are classified as aeolian formed landforms along the coast of New Zealand. The distinction between active and stable dunes is influenced by the development of scrub vegetation and by the appearance of soil horizons in stable dune systems (Singers and Rogers, 2014). The five classifications are separated by temperature and biographic pattern. This Classification also includes dune slacks and deflation hollows that are temporary wetlands. These are recognised by Singers and Rogers (2014) as potentially being its own ecosystem classification.

Due to the National Ecosystem Classification system's categorisation by physical and environmental drivers, many stabilised back dune forests are classified as a different category as it is influenced by zonal ecosystem drivers. Additionally, fixed or relict dunes are excluded from this Classification and are also classified as a zonal ecosystem (Singers and Rogers, 2014). Similar to the PNAP surveys, this ecosystem approach allows the forested areas back dunes to be given an ecological weight in accordance with the specific drivers and botany of the area.

1.2.4 Adoption of the National Ecosystem Classification by Auckland Council

Indigenous Terrestrial and Wetland Ecosystems of Auckland Classification (2017)

Auckland Council has classified the Auckland region into 36 terrestrial and wetland ecosystems. This work was based upon the previously mentioned National Ecosystem Classification system produced by the Department of Conservation (Singers et al., 2017). Adoption of the National Ecosystem Classification System has spread across multiple regional authorities, including Auckland and provides a consistent methodology for comparisons between various ecosystems. The system was developed to meet the requirements of goal 3 of the New Zealand Biodiversity strategy to "maintain and restore a full range of remaining habitats and ecosystems" (Singers et al., 2017). The classification system allows targeted ecosystem protection and assessment and monitoring of key environmental drivers and threats to ecosystem health.

Two of the five dune ecosystems defined by the National Ecosystem Classification are present in the Auckland region: Spinifex, Pingao, grassland/sedgeland (DN2) and Oioi, Knobby Club Rush Sedgeland (DN5), see Table 1. Karekare is classified as DN2 in both the national and Auckland-based ecosystem framework. The DN2 Classification includes active sand dunes, where dominant ecosystem drivers include salt winds, periodic drought, high surface temperature and low nutrient availability (Hesp, 2000). Dunes consist of a variety of drought-tolerant plants. Dune systems have a successional pattern as the dune over time.

Table 1: Ecosystem Frameworks of active coastal sand dunes found in the Auckland region (Singers & Rogers, 2014).

PRIMARY ECOSYSTEM DRIVER: FREQUENT GEOMORPHIC DISTURBANCE	**SECONDARY ECOSYSTEM DRIVER: TEMPERATURE**	**TERTIARY ECOSYSTEM DRIVER: MOISTURE**	**QUATERNARY ECOSYSTEM DRIVERS: LANDFORMS AND SOILS**	**ECOSYSTEM UNIT**
Erosion and accretion of sand from wind ablation [Active coastal sand dunes]	Warm to mild temperate	Semi-arid to humid	Dunes with raw sandy soils in association with atmospheric salinity (e.g. spume and salt-spray)	DN2: Spinifex, pīngao grassland/ sedgeland
Erosion and accretion of sand from wind ablation [Active coastal sand dunes]	Warm to cool temperate	Semi-arid to humid	Dune plains (including deflation hollows, dune slacks, damp sand plains and stream terraces) and exposed coastal hill slopes with raw sandy soils	DN5: Oioi, knobby clubrush sedgeland

Threats to the DN2 ecosystem include human trampling, rabbits, bike or motorbike disturbances. Active dune systems are highly mobile, and previous dune stabilisation programmes used invasive weeds such as Marram grass and Lupin that pose severe threats to the native flora. The regional IUCN threat status of this ecosystem is endangered.

1.3 Techniques for Dune Monitoring

The previous section detailed the national and regional surveys conducted to classify New Zealand's dune ecosystems. A range of different sampling techniques and data sets were used to classify locations within the survey structure. Many additional datasets and ancillary information now supplement traditional field sampling methods (Singers & Rogers 2014). Resources such as the Land Cover Database, S-map for soil and properties and climate are all valuable tools for monitoring programmes. In addition, there is a wide variety of publicly available satellite imagery covering a large proportion of the country.

1.3.1 Remote Sensing

Remote Sensing has been defined as "the art, science and technology through which the characteristics of objects/targets either on, above or even below the Earth's surface are identified, measured and analysed without direct contact existing between the sensors and the objects or events being observed" Awange & Kiema, (2013). This definition is used in this thesis as it embodies the sensor or technology used and the end-user's underlying scientific principles and interpretations. Although all remote sensing projects should be understood in this manner, it is crucial to recognise the sensor or technology as a tool to aid a project's goals. Therefore, the methodology, tools and objectives will vary greatly depending on the objects or phenomena observed the aims of the project.

Remote Sensing has vast applicability in ecological studies and can add supplementary information to traditional ground-based methodology, which is a lot more time-consuming and risks damage to the observed site (Gruszczynski et al., 2017). Repeatability for short- and long-term monitoring is another potential advantage of Remote Sensing methodologies (Hugenholtz et al., 2012). It is often not viable to set up permanent ground sampling plots in

environments that can be highly dynamic (Kaliraj et al., 2017). Using Remote Sensing-based algorithms, monitoring of a defined area can be achieved with high levels of accuracy (Krapivin & Shutko., 2012). Ecosystem response and time-series analysis is now an established field in remote Sensing and a favoured method for many projects (Tuna et al., 2020).

Remote Sensing Resolutions

When assessing the methodology of a Remote Sensing project, there are four main resolution variables to consider: spectral, spatial, temporal and radiometric resolution. Spectral resolution relates to how reflected energy is measured and divided by an image sensor. A standard camera will measure only visible light (red, green and blue wavelengths). The traditional camera lens does not have a discrete lens to define red, green and blue and therefore interpolates the data values to provide the end-user with an image representative of the red, green, blue image values. Sensors used for remote Sensing are engineered only to read a specific wavelength range of the electromagnetic spectrum. For example, three discrete sensors record visible light (red, green and blue) on the MicaSense RedEdge sensor. The sensor used for blue reflectance will only capture reflectance between 465 – 486 nanometer (nm) bandwidths, while the green sensor will only record 550 – 570nm reflectance.

Spectral Resolution

The number of bands recorded by a sensor platform will define the spectral resolution. In Remote Sensing, there are three main categories of spectral resolution: panchromatic, multispectral and hyperspectral. Panchromatic refers to a single band reflectance output. In Remote Sensing, panchromatic images are related to greyscale (black and white) imagery

where a single reflectance value is used for the whole range of the visible light spectrum. Multispectral imagery refers to multiple discrete bands, usually between 3-10. Finally, Hyperspectral remote sensing platforms can have hundreds of contiguous spectral bands (Mateen et al., 2018).

Most multispectral sensors used in remote Sensing consist of non-contiguous bands, which leave gaps in the data set. The hyperspectral sensor can provide narrow-band, contiguous bands. For example, the Hyperion sensor of NASA'S Earth Observing Satellite (E0-1) has 242 spectral bands, which can record both visible/near-infrared, VNIR, (400-1000 nm) and shortwave infrared, SWIR, (0-2500nm) (Chutia et al., 2016). However, due to the overlay of VNIR and SWIR, 22 bands are removed, leaving 220 bands used for analysis. There have been multiple studies using the enhanced spectral resolution of hyperspectral imagery on a wide range of environments from soil composition (Golubiewski and Wessman, 2010), minerals (Lévesque and Staenz, 2008) and vegetation and weed mapping (Zhang et al., 2012).

Spatial Resolution

Spatial resolution in Remote Sensing is defined as the linear dimension on the ground surface of an individual pixel (Wang et al., 2012). The spatial resolution will significantly impact remote sensing studies as, in general, only objects larger than the minimum mapping unit (MMU), usually 2x2 pixels, can be observed with any degree of accuracy. However, not all studies will benefit from a very high spatial resolution. For example, having a high spatial resolution may reduce the area coverage of a project.

Radiometric Resolution

Radiometric resolution refers to the dynamic range of the data or the amount of different values that can be recorded for each spectral band (Wang et al., 2012). Radiometric

resolution is measured in bits. For example, an 8-bit data source will record a digital number between 0-255 (2^8 = 256 different numbers). A 10-bit data source will have digital numbers from 0-1023 (2^{10} = 1024 different numbers). The higher the radiometric resolution, the better the sensor will differentiate between small changes in reflectance.

Temporal Resolution

Temporal resolution refers to the frequency of repeat sampling missions (Baghdadi & Zribi, 2016). For satellites, temporal resolution refers to the time it takes for a platform to complete an entire orbital cycle (16 days for Landsat-8, for example). The temporal resolution can be tailored to the given project for other remote sensing applications such as aerial photography and UAV imagery. The choice of temporal resolution will need to depend greatly on how dynamic the site is and the aims and goals of the analysis.

The four resolution variables need to be considered holistically for any remote sensing project. For example, there is often an inverse relationship between spectral and spatial resolution. The same trade-off exists in orbital satellites for spatial resolution and temporal resolution. Therefore, the choice of sensor and platform is perhaps the most crucial step before undertaking any mission as it will dictate what is achievable relevant to the project's outline.

1.3.2 Remote Sensing of Coastal Sand Dunes

There are a wide variety of sensors and platforms that have been used for Remote Sensing of coastal environments. There are two main types of platforms: space-borne (i.e. satellite platforms) and air-bone (both piloted planes/helicopters and Unmanned Aerial Vehicles (UAVs)) (Müllerová et al., 2013). The decision to use a specific platform or combination of platforms will depend on the goal and spatial scope of the project. Regional and National-

scale monitoring will rely primarily on Satellite imagery in combination with aerial imagery (Whitehead 2014). Small-scale/local analysis will use predominantly aerial imagery and UAVs (Gruszczynski et al., 2017; Hugenholtz et al., 2012).

In recent years there has been an increased focus on the use of UAVs for Remote Sensing studies in a wide range of environments, for example, forest ecosystems (Zahawi et al., 2105), agriculture (Tsoros et al., 2019), Areas prone to landslides (Rossi et al., 2018) etc. In particular, UAV-based coastal studies have been carried out in many different locations globally (Scarelli et al., 2017; Suo et al., 2019 etc.). UAVs are suited for coastal environments because coastal systems are geomorphologically active and have many drivers for geomorphic change, including seasonal and event-based (storm) causes (Kaneko & Nohara., 2014). In addition, UAVs can be rapidly deployed and have been employed to detail and evaluate the effects of destructive events such as large storms in a coastal setting and landslides for inland areas (Ruessink et al., 2018). UAVs have also been used for illustrating long-term changes with increased temporal resolution. The expense of aerial surveys using an aeroplane or helicopter is much greater than a UAV; therefore, multiple flights every year can be conducted using UAVs (Turner et al., 2016). However, the aerial extent is more limited, and therefore locations of ecological or historical significance need to be targeted (De Giglio et al., 2017).

Vegetation classification using remote sensing methods has been widely employed in many ecological studies (Xie et al., 2008). Vegetation classification uses computer-assisted machine learning to automatically classify an area into different classes (Jensen, 2000). There are two main types of Classification – supervised and unsupervised. Unsupervised Classification is when the computer runs a set of algorithms to assign individual pixels into a class with similar characteristics. Supervised Classification is where the user inputs a series of training values representing a class with similar attributes. Supervised Classification uses

pre-existing information, and the algorithm then uses the defined characteristics to assign a pixel to a specific class (Bolyn et al., 2018). In general, Unsupervised Classification is only used as exploratory information to understand spectral differences of a study site. In most studies, there are goals and objectives relating to specific vegetation classes that the user is trying to determine, for example, a specific invasive plant species or a vegetation class of significant ecological value.

A relatively new sector of remote sensing classification is Object-Based Image Analysis (OBIA). OBIA varies from traditional pixel-based methods principally by adding an additional process, image segmentation, before the Classification is undertaken (Ma et al., 2017). Traditional pixel-based classifications assign an individual pixel to a class category. However, OBIA segments the image into objects with similar attributes, a series of neighbouring pixels belonging to a single group/object (Li et al., 2014). Once the segmentation and objects are created, the classification algorithm is run per object, not per pixel.

OBIA is a very useful technique for Very High Resolution (VHR) data. An object of interest, for example, an individual tree, may have many pixels. Traditional pixel-based methods may create a salt-and-pepper effect, whereby multiple different classes are present within a single feature (Song et al., 2020). OBIA aims to classify individual features as a single object reducing the amount of misclassification within the boundaries of the feature. UAVs produce VHR data; therefore, there has been an increase in the amount of UAV-based studies using OBIA instead of traditional pixel-based classifications (Baatz et al., 2000).

However, UAV based and OBIA based studies are still a relatively new field of study, and there remains a lot to learn and develop to create a list of best practices for UAV-based Remote Sensing studies. Therefore, this study aims to compare the differences between pixel-

based and OBIA methods and provide guidance on the advantages and limitations of using UAVs and OBIA-based methods for environmental monitoring of Coastal Environments.

1.4 Goals and Objectives of this Study

- Compare and contrast pixel-based and OBIA classification methods advantages and limitations for analysis of high-resolution data.
- Provide a Case study on the effect of seasonal/temporal variance on UAV-based vegetation classification.
- Assess the effectiveness of UAVs for use in Vegetation monitoring and Classification.
- Create a detailed workflow and list of best practices for using UAVs for vegetation classification.
- Evaluate the advantages and limitations of present technologies and processes.

1.5 Study Site

Karekare Beach is located on the West Coast of Auckland, north of Whatipu Scientific reserve and south of Piha beach (see Figure 1). Karekare is classified as a DN2 Ecosystem (Spinifex, pingao grassland/sedgeland) in the national and Auckland-based ecosystem framework. The DN2 Classification includes active sand dunes, where dominant ecosystem drivers include salt winds, periodic drought, high surface temperature and low nutrient availability (Hesp, 2000).

Figure 1: Map of Karekare Sand Dunes study site

Threats to the DN2 ecosystem include human trampling, rabbits, bike or motorbike disturbances. Active dune systems are highly mobile; previous dune stabilisation programmes used invasive weeds such as marram grass and lupin that pose severe threats to the native flora. The regional IUCN threat status of this ecosystem is endangered.

Karekare has been classified as a high priority site for weed management by Auckland Council (Craw, 2015). The stream, coastline, and bush edges were significant in the weed management plan (Craw, 2015).

1.5.1 Contemporary Vegetation Monitoring of Karekare Beach

Auckland Council conducted a systematic vegetation survey of Karekare beach in late 2017 (Auckland Council 2018, unpublished). The sampling consisted of five transects perpendicular to the coastline with sampling spacing ranging from 20 to 30 metres. Circular sampling plots with a 2m radius were set up with the species and percentage cover recorded at each plot. During this study, Dominant vegetation species included Spinifex in the foredunes. The mid to back dunes were dominated by species such as Muelenbeckia complexa, Ficina nodosa, Lupinus arboreus, Ozothamnus leptophyllus and herbland species, including Senecio skirrhodon and Lachnagrostis billardierei (Auckland Council 2018, unpublished). A total of 44 different species were identified in the survey.

1.5.2 Geological setting

The geology of Karekare and surrounding west coast beaches comprise of the Waitakere Group consisting of volcanogenic rocks and underwater sediment created in the early Miocene, which were then uplifted, see Figure 2 (Hayward, 2017). Embayment filling and shoreline propagation began around 6500 years ago, resulting in Karekare and adjacent west coast beaches (King et al., 2006). Karekare's sand systems contain mineral-rich black sand with a large proportion of heavy iron ores and lighter quartz and feldspar ores (Hamill & Balance, 1985).

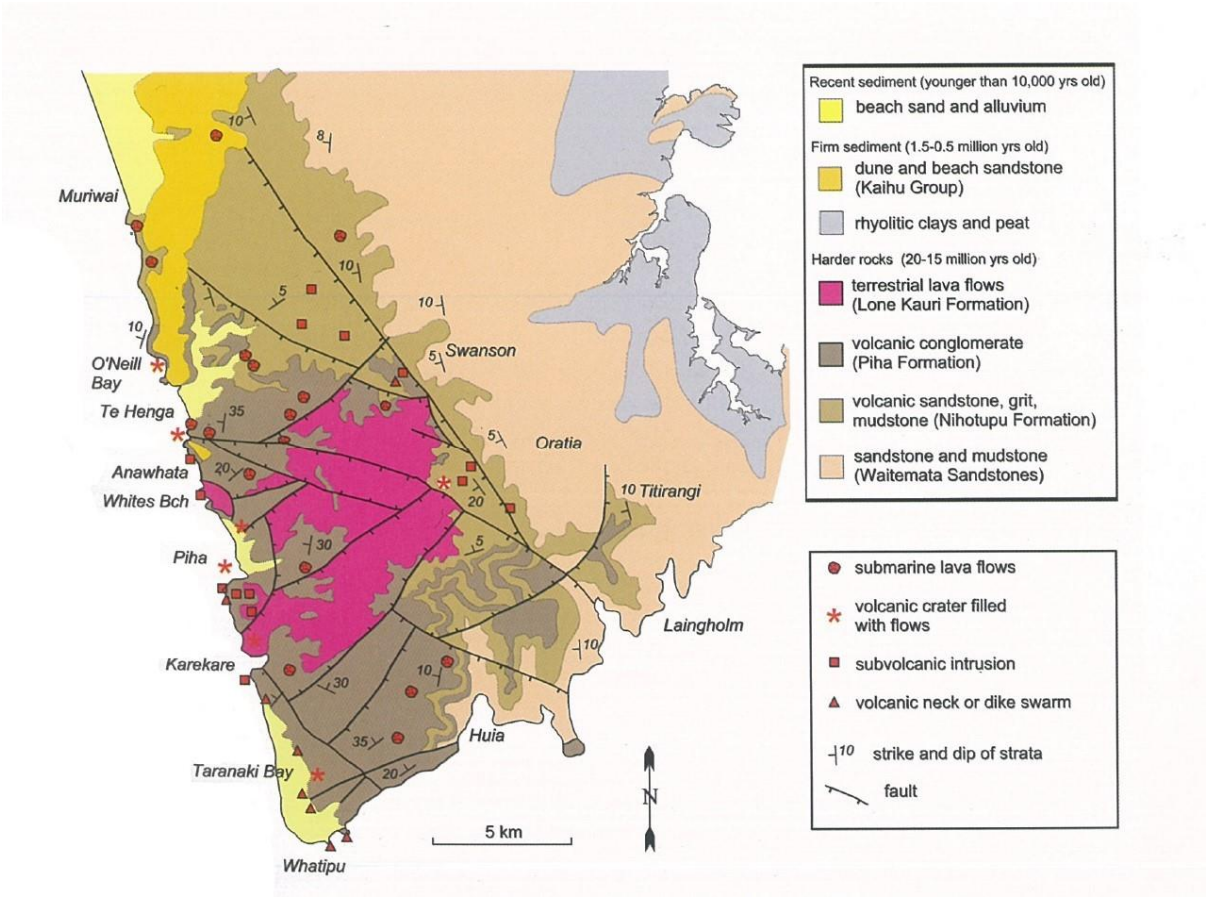

Figure 2: Simplified Geological Map of West Auckland (Hayward, 2017).

1.5.3 Karekare historic Sand Dune erosion and propagation

In Blue & Kench's (2017) paper, it was found that the Karekare study site had minor shoreline retreat; the mean dune toe was displaced 22 metres inland from 1940 to 2010. Erosion was most rapid between 1940 and 1960 at 2.2m/yr. However, between 1980 and 1988, there was a period of rapid propagation at 4.0m/yr, followed by erosion in 1988-2003. Finally, between 2003 and 2010, propagation of 4.5m/yr resulted in the recovery of tha majority of dune loss since 1980.

2. Methods

2.1 Diagram of the eight steps undertaken in the project

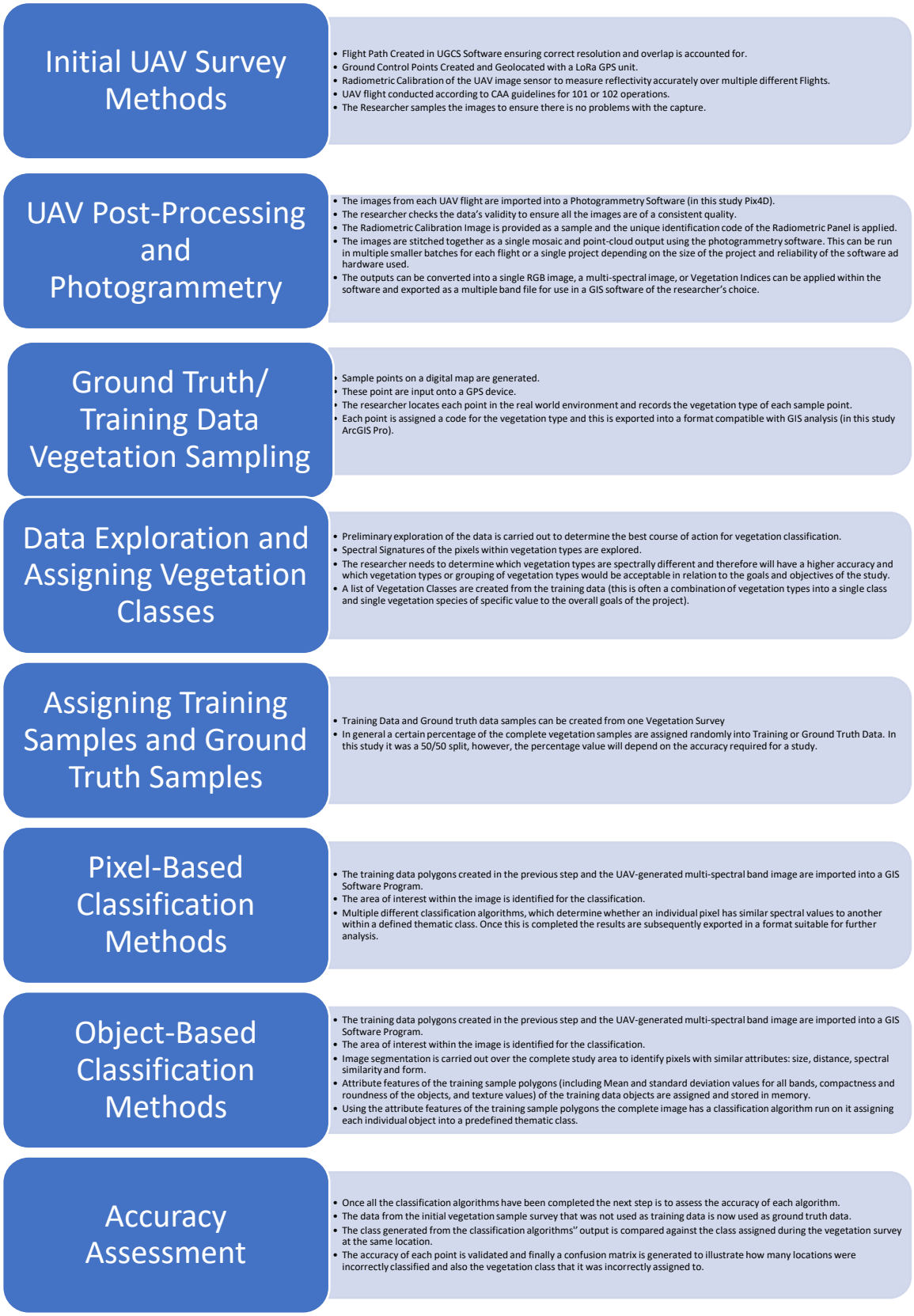

Figure 3: Diagram of the Key steps for UAV Vegetation Classification

2.2 Initial UAV Survey Methods

2.2.1 Flight Mission Planning Software - Universal Ground Control Software (UGCS)

UGCS was used for flight planning. Therefore, it is essential to modify the parameters and flight pattern to suit the project's goal. UGCS has various UAV platform setups, including the Phantom 4 Pro UAV platform with the MicaSense Red Edge sensor used in this study. By selecting the correct UAV platform, the software can create flight plans relatively autonomously. Flight resolution, image overlap, Flight area and flight pattern (single or double grid) were the only user imputed variables. Due to the added weight of the Red Edge sensor, flights were limited to less than 15 minutes as opposed to the 25 -27 minutes advertised for the Phantom 4 pro without the Red Edge. A 1-metre resolution Digital Elevation Model (DEM) produced by Auckland Council in 2015 was input into UGCS as the baseline elevation. The inclusion of the DEM to the flight programming allowed UGCS to maintain a consistent elevation (80 metres) over the study area and adjust to the changing topography. The goal of retaining this elevation is to reduce artefacts that can occur if the UAV was operated at a defined height from the take-off point, not taking into account the local topography

A total of six flights were created in the UGCS software. The advantage of using flight-mission software is the flights can be easily replicated. For example, this study used the same flight plans for the November and March flights as the UAV platform, and sensor remained unchanged. Therefore, the pre-flight planning allows for change detection of the area with minimal set-up once the initial flight missions have been created.

2.2.2 Ground Control Points (GCPs)

GCPs are points that are manually recorded by GPS units with greater accuracy than the UAVs internal senor. GCPs need to be easily identified in the output UAV images. GCPS are used to correct inherent positioning errors associated with the internal sensor of the UAV,

therefore increasing real-world accuracy. GCPs can be manmade or natural, for example, edges of roof houses or distinctive rock outcrops. The choice of GCP will depend on the resolution of the imagery, accuracy of GPS survey equipment and goal of the project. This study aimed to look at 3D dune structure and vegetation mapping at a resolution of 5cm. Given the previous requirements having very accurate GCPs was important. The natural landscape of the dunes was highly dynamic, with very little permanent structures that could be used as a GCP.

Therefore, the GCPs were created from vinyl mats with a black and white checker pattern. The pattern allowed for easy identification of the central point. The vinyl mats consisted of four squares, 15cm in length. The total dimensions of each mat were 30x30cm. Vinyl mats were chosen as they are waterproof and relatively lightweight for transportation to the study site. Each square of the ground control points was also greater than the imagery's minimum mapping unit (10x10cm). The mats were anchored to the ground with tent pegs on each mat corner to avoid movement before the flight. As per the Auckland Council's research permit stipulations, ground control points were removed the same day as the UAV flights.

In remote sensing studies, a minimum of five GCPs is required as a baseline for creating georectificed orthomosaics. In order to cover the complete area of the Karekare study site, six flights were required. This study was concerned with assessing the ability of the photogrammetry software to perform radiometric calibration and orthomsoaic generation. Therefore, radiometric calibration was applied to each project in isolation from another flight. To create six separate projects, five GCPs were placed within each of the six flights. The layout represented a five dice pattern, a GCP in each corner and one in the middle. Each GCP was measured with a fixed signal (0.05-0.012m RMS) using the Emlid Reach RTK GPS unit. The fix and hold setting was used; this averages all readings over a fixed time, one minute for each GCP.

2.2.3 Real-Time Kinetic Surveying Set-up Procedures

An Emlid Reach RTK unit was used for both the vegetation survey and the recording of GPS points for the UAV flight. RTK allows centimetre level accuracy to surveying missions. The use of real-time RTK base stations which link back to RINEX stations is common in higher-precision survey missions. While this is an effective methodology for surveying, the cost of these base stations is very high.

For this study, the RINEX corrections were done post-processing in the lab instead of in the field. The first step was to set up a base station reading and record its position for eight hours. Once the logging was completed, the raw data logs were post-processed to the nearest RINEX station (Auckland Whangaparaoa base station 55km away). This methodology resulted in the creation of a known survey point that has been corrected, and GPS drift and internal sensor inaccuracies have been mitigated. Once the point was created, a tent prong was placed at the centre point of the base station, and the resulting coordinates were manually entered into the reach unit. The antenna height was also recorded and kept consistent throughout all subsequent surveys. This methodology created a known survey point similar to the NZ standard geodetic markers in New Zealand. In addition, this methodology allows RTK surveys of remote locations without known geodetic markers or an expensive real-time base station setup.

The topography of the region dictated the choice of the known survey point. Long Range Radio Signal (LoRa) allows for a base to rover connection that can span more than 1 km. Even though LoRa signals are characterised by their long wavelength, hills can still degrade signal quality. To counteract the influence of topography, the survey point chosen was a relatively unvegetated high foredune. The point was selected to reduce the impact of reflected

GPS signals from nearby objects and create a clear line of sight from the base to the rover units.

2.2.4 UAV Flight Mission Safety and Quality Protocols

Two UAV flight missions were carried out, one on November 7th, 2018 and another on March 28th 2019. Six flights were completed for each mission between 10:30 am and 3:00 pm. Flights were completed during these hours to reduce shadow effects from the oblique angle of the sun. Ideal weather conditions for UAV flights are clear sky, low wind and the sun angle being as close to nadir as possible. On the day of both flight missions, there was low wind. However, there was intermittent cloud cover that varied from flight to flight.

All flights were completed with a designated operator and a spotter to ensure two sets of eyes were always focused on the vehicle while in flight. A clear unpopulated area with an adequate line of sight was chosen as the take-off and landing point. This area was signposted to make the public aware of the purpose of the flight and avoid any distractions and potential dangers from public intervention while flying the UAV. Before and after each flight a checklist assessment of the platform and software was carried out to mitigate any potential risks for example propeller damage, errors in syncing with the drone and the remote controller, camera errors, insecure battery placement and structural damage to the UAV.

UAV health and safety protocols were followed according to both Auckland University of Technology and Civil Aviation Authority (CAA) guidelines for UAV missions. These included filing a UAV con-op and health and safety report assessing any risk prior to the field missions. NOTAMS detailing any activity within the defined air space were checked the morning of each flight mission. All UAV flights were operated within the CAA 101 guidelines and the entire study site was within unrestricted airspace.

A reference panel needs to be used for radiometric calibration to be carried out. A factory calibrated MicaSense reference panel was used with known values for all five bands the RedEdge sensor records. Immediately before and after each flight, a photo was captured using the RedEdge sensor. To minimise external variabilities a set of protocols following were observed for each capture. The following protocols represent best practice methodology for radiometric calibration recommended by Pix4D support:

- The target is to be level with the ground and not at an angle.
- The target should be facing North to avoid artefacts when the sung angle correction algorithm is applied.
- The target should not be in shadow with no reflection of surrounding objects visible.
- The calibration target should not be over/under exposed in any of the bands.).
- For images taken with the target on the ground, the camera should be around 1 meter from the target and not facing the sun.
- Complete a Quality Check of the camera metadata to ensure the correct GPS time and location are recorded for the flights.
- Take multiple captures of the calibration target to get at least one high-quality calibration image.
- Check the calibration target captures on-site to ensure the images are not over/underexposed.

2.3 UAV Platform and Sensor

The UAV platform included a Phantom 4 Pro with a MicaSense RedEdge sensor (see Table 2 and Figure 4 for more detail on the RedEdge sensor). The platform was also outfitted with a

sun luminance meter to account for changing laminations during the flight. Luminance values are automatically recorded in the EXIF files of each capture and used in the post-processing steps.

Table 2: RedEdge Sensor Bands and Wavelengths

Band/Channel	Wavelength
1. Blue	465-485nm
2. Green	550-570nm
3. Red	663-673nm
4. Red Edge	712-723nm
5. Near Infrared	820-860nm

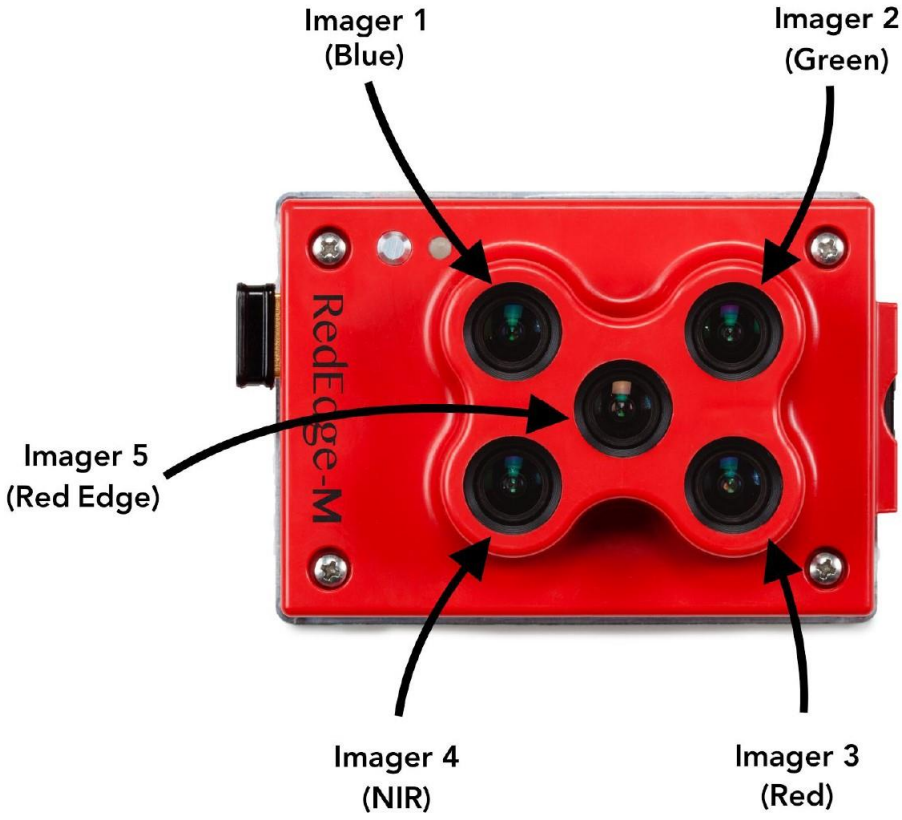

Figure 4: Red Edge Sensor Schematic view (Pourazar et al., 2019)

2.4 UAV Post-Processing and Photogrammetry

2.4.1 Photogrammetry

Processing of the UAV imagery was undertaken in Pix4DMapper. This software uses photogrammetry methodology to "stitch" together multiple images to create an orthomosaic.

Parameters used in Pix4D Processing

Pix4D offers a variety of customisable parameters that will influence the final result of the imagery. The settings used will vary from project to project in accordance with the quality of the imagery recorded and the overall goals of the operation. Factors influencing which settings should be used include: image overlap percentage, resolution of the camera, the altitude of the flight, illumination conditions, topology of the region, density of the As the flights in this study consisted of a cross-grid pattern (see chapter number and letter of UGCs flight plan) with 60% overlap it is possible to achieve a highly detailed digital surface model from the point cloud without simplification. Therefore, the parameters used in Pix4D Mapper were consistently the highest quality with the least amount of generalisation or interpolation. However, this significantly increased the processing time for all tasks. As this project's purpose is to be used as a case study, the highest quality parameters were chosen as the quality was given greater importance than the time taken for processing.

The first processing stage involves organising the images into meaningful folders for ease of use within the Pix4D Mapper software. The MicaSense RedEdge sensor will automatically catalogue the images into folders on the SD card. New folders will be created for each flight, and when manually pressing the camera button for calibration, a new folder will also be created. This makes processing streamlined; however, it is important to double-check the folders have been created correctly before analysis. Checking the EXIF file of each photo and

matching it with the times manually recorded when the flight took place is easy to determine if the capture is correct. However, even if the capture is accurate, images often are not useful and could adversely affect the final result. These could include using data from cancelled flight missions, blurred images or not including the entire flight mission if it was split over multiple folders.

For the missions captured, the MicaSense sensor captured images every 2 seconds from the moment it was synced with the Phantom 4 Pro. Therefore, all images from the take-off point to the first survey and from the final survey to the landing point needed to be deleted. To remove these pre and post-survey images from the images that will be processed. The images were imported into Pix4D and visualised using the map view function. This allowed the identification of photos represented by a GPS point on the map, not within the survey grid created in UGCs. Next, the images not in the survey were moved to a separate folder leaving only the photos within the survey to be used and then reloaded into the Pix4D mapper as a new project.

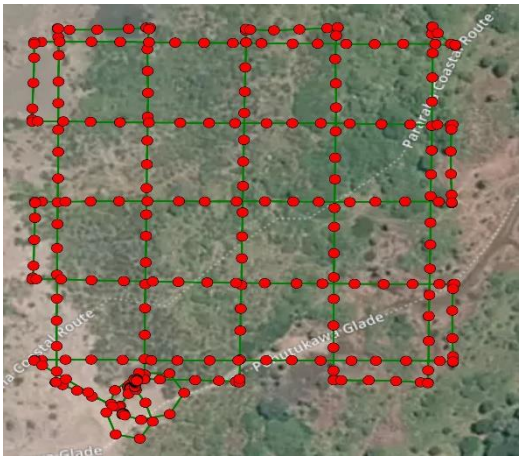

Figure 5: UAV flight plan of Karkare. Red Dots represent the images collected and the green lines indicate the flight path.

Photogrammetry calculations are influenced by various parameters associated with the camera rig used, including focal lens, sensor size and radial distortions between individual cameras (Pix4D, 2018). Therefore, before completing the analysis in any photogrammetry

program, the camera properties must be explicitly adjusted to the model that was used. Suppose the software does not recognise the camera used and provides generic values. In that case, these can be manually altered by using documentation from the camera model and adjusting the parameters specific to the model used. If generic parameters are used, it will increase the likelihood of distortion and artefacts in the final model. Pix4D mapper includes a wide variety of camera model pre-sets, and the correct RedEdge model M type was automatically generated from the EXIF file when the photos were loaded.

All photogrammetry software packages follow three core processes to create an output. These processes are initial processing, point cloud and mesh generation and DSM, Orthomsoaic and Index model generation. All three processes have a wide variety of parameters that can dramatically alter the quality of the final model. While there is no turnkey solution for optimal settings, Pix4D provides in-built settings for categories such as multispectral studies of the natural environment, urban 3-D mapping, etc. However, these settings are only a guide, and for optimal results changing the parameters to suit the projects design and goals is needed. The flight plan created allowed all settings to be adjusted to their maximum resolution/quality pre-sets due to the overlap and grid-corridor flight pattern.

The initial settings used a double image size for generating the key points used for image matching. If the images did not have significant overlap, or there was little difference between images, this value can be reduced. Reducing the image size increases the likelihood of image matching but decreases results in a reduction of detail to the model. An example of a situation where image scale reduction would be a better choice would be mapping a relatively uniform, densely vegetated pine plantation. Aerial grid or corridor algorithms were used as opposed to a free flight which can be used if a flight mission was not created before the flight. For photogrammetry purposes, it is always advised to use flight mission software rather than free flight modelling. However, there may be situations where there is little

known of the area flown, or the GPS signal is very low where free flight may be the only viable option.

The initial processing stage is the most CPU and RAM intensive step of the photogrammetry process. Therefore, projects with many photos can be split into subprojects for the initial processing stage and then combined for the next two steps (Pix4D, 2018). For this study, a powerful consumer-grade computer was used to process (AMD Ryzen 2700x eight-core CPU, 32gb of ram and a 1080ti Nvidia Graphics card). However, even with this high spec computer, the processing was needed to be restarted multiple times to complete the processing. The initial processing took around four hours to calibrate the complete project of 6785 images. After that, the Point Cloud generation took approximately four hours, the 3D mesh two hours and the final stage three hours of processing.

The previous initial processing stage uses both the internal GPS coordinates and image matching to generate to align the images. To achieve an accurate geolocated model ground control points are added to the project then manually georeferenced. The ground control points measured by the Emlid Reach Unit were added to the GCP manager map. The software estimates where each point could be, and the user will manually drag the cursor to the centre point of the GCP, where the measurement was recorded. Due to the image overlap, multiple images will have the GCP square visible and adjustment

For the software to estimate GCP coordinates, both the GCPs and orthomsoaic needed to be in the same coordinate system. Emlid Reach units only record coordinates in WGS84 and height elevations represent ellipsoid heights rather than geoid height as metres above mean sea level (msl). To create a Digital Elevation Model that uses Mean Sea Level (msl) as a base point, all coordinates need to be converted. The Geoid Height Calculator created by UNAVCO was used for the vertical corrections.

The next stage of the processing involved generating a point cloud and 3D textured mesh. There are various parameters that can be used that will influence the density and resolution of the point cloud. For this study, maximum resolution (original image size and high point density) was chosen. A 3D textured mesh was also generated using the highest resolution.

The final stage builds many of the outputs required for UAV image analysis (orthomosaic, Digital Surface Model and Reflectance maps). Before creating the orthomsoaic and reflectance maps, radiometric calibration needs to be performed to allow normalised reflectance values between 0-1 and time-series analysis of multiple UAV reflectance maps.

2.4.2Radiometric Calibration

Radiometric calibration was required for both time-series analysis and the accurate creation of vegetation indices. Pix4D mapper has a tool for radiometric calibration that has been designed to work in unison with MicaSense products.

The formula for computing the spectral radiance L from pixel value p, is:

$$L = V(x,y) * \frac{a_1}{g} * \frac{p - p_{BL}}{t_e + a_2 y - a_3 t_e y}$$

Where,

- p is the normalized raw pixel value
- p_{BL} is the normalized black level value (can be found in metadata tags)
- a_1 a_2, a_3 are the radiometric calibration coefficients

- V(x, y) is the vignette polynomial function for pixel location (x, y). See “Vignette Model” section.
- t_e is the image exposure time
- *g* is the sensor gain setting (can be found in metadata tags)
- *x, y* are the pixel column and row number, respectively
- *L* is the spectral radiance in $W/m^2/sr/nm$

Before and after each flight, an image of the calibration panel was captured to calculate reflectance relative to the ambient light conditions. Each panel is factory calibrated with defined values for each spectral band recorded; see Figures 6 and 7 for reference. In addition to the calibration panel, the UAV has a sunlight sensor attached to document changing luminance values during the flight mission.

Figure 6: Image showing the identification of calibration panel. The reflectance value is manually imputed from the unique QR identifier of the panel.

Panel Values

```
RP03-1731212-SC
--------

RedEdge
--------
blue    0.55
green   0.55
red     0.54
nir     0.49
re      0.53

Sequoia
--------
green   0.55
red     0.55
nir     0.49
re      0.53
```

Figure 7: Unique values of reflectance used for the panel

2.4.3 Vegetation Indices

The MicaSense RedEdge sensor records five spectral bands; vegetation indices were used as supplementary data for the final classification algorithms. Vegetation indices are algorithms applied to spectral bands used as analogues for various vegetation processes and nutritional conditions. The most commonly used vegetation index is the Normalised Vegetation indices (NDVI). The equation for NDVI is (NIR – Red) / (NIR + Red). This Vegetation Index is used to estimate chlorophyll production. Chlorophyll reflects near-infrared but absorbs comparably more red light. Therefore, the NDVI equation is used as an analogue for plant health as chlorophyll is the byproduct of the photosynthesis process; therefore, the more chlorophyll in a plant, the more productive the plant is.

NDVI is one example of vegetation indices. However, many other algorithms can be used as additional information for differentiating vegetation species. This study used a total of ten different vegetation indices. Table 3 shows the vegetation indices used in this study the vegetation indices chosen were adapted from Hatfield and Pruegar's Study (2010). These vegetation indices will be used in the classification map and the change detection analysis between the two flight missions. In addition, vegetation indices have large seasonal variability and understanding the temporal dynamics of the vegetation is essential to understand the influence seasonality has on the final Classification.

Table 3: Vegetation Indices and the waveband equations used in this study, adapted from Hatfield and Pruegar (2010).

Vegetation Index	**Waveband Equation**
Normalised Difference Vegetation Index (NDVI)	(NIR-Red)/(NIR+Red)
Ratio	NIR/Red
Green NDVI	(NIR- Green)/(NIR+Green)
RedEdge NDVI	(NIR-RedEdge)/(NIR_RedEdge)
Soil Asjusted Vegetation Index (SAVI)	(NIR-Red)(1+L)/(NIR+Red+L)
Enhanced Vegetation Index (EVI)	2.5(NIR-Red)/(NIR+6Red-7.5 Blue +1)
Normalised Pigment Cholorophyll Ratio Index (NCPI)	(Red-Blue)/(Red+Blue)
Chlorphyll index (Green)	(NIR/Green)-1
Chlorphyll index (Red Edge)	(NIR/Red Edge)-1
Plant Sensescence Reflectance Index (PSRI)	(Red-Green)/NIR

Calculating Vegetation Indices in Pix4D

Computer-generated vegetation indices are calculated for every individual pixel of a scene. Before the vegetation indices are calculated, each pixel in the scene will have a value for the five spectral bands recorded by the sensor (blue, green, red, NIR and Red Edge). For example, the Ratio index will take the NIR reflectance value and divide it by the Red reflectance value. If the NIR value was 0.6 and the Red value was 0.2, the ratio would be 3 for that pixel (0.6/0.2 = 3). Pix4D Mapper allows the calculation of vegetation indices using an in-built function to allow band math to be performed, see Figure 8. It is also possible to

compute vegetation indices in other software programs such as ENVI. The Band math function in ENVI is used to calculate the vegetation indices using the reflectance data output by Pix4D Mapper. The outcome of using either of these methods is the same, and the choice will be determined by user preference.

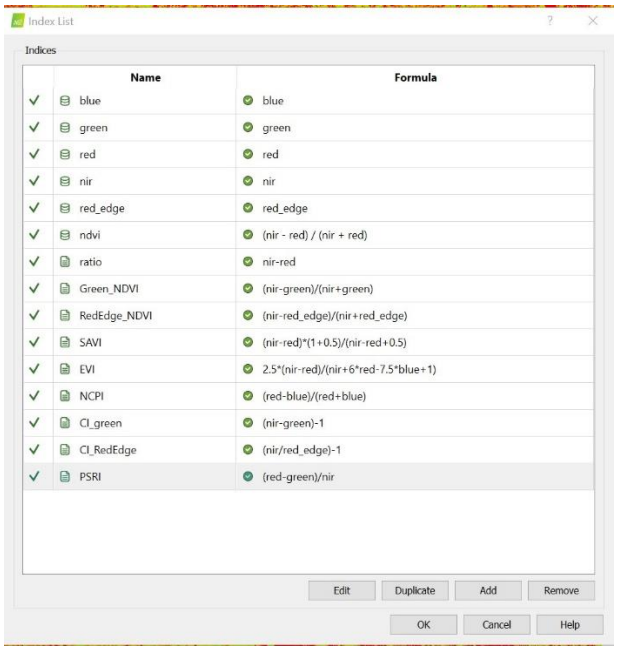

Figure 8: Vegetation Indices input using band math within the Pix4D software.

2.4.4 Final Output of PIX 4-D

Once radiometric calibration and vegetation indices have been created. Final exports such as orthomsoaic, vegetation maps and digital surface models are exported to a suitable format ready for analysis. For this study, making sure each orthomsoaic and vegetation index was exported as a lossless TIFF file was important so no compression artifacting can occur for formats such as JPEG2000.

2.5 Ground Truth/ Training Data Vegetation Sampling

Sampling design is an essential factor in any ecosystem study. For this study, a stratified random sampling strategy was employed. Two stratified zones were created for the study site of Karekare Beach, the active foredune area (consisting primarily of the sand-binder species pingao and spinifex) and the established mid-back-dune area. A total of 800 points of the mid to back dunes were created and 400 points for the foredune zone using the random points generator in QGIS. While the foredune area does not represent 1/3 of the total area, the choice to have a greater percentage of points was governed by the importance of key sand binders such as Pingao and Spinifex and to test if there was any encroachment of exotic weeds such as tree lupin on this area.

To mitigate against changes to the highly dynamic active dunelands, vegetation sampling was conducted within a two-week time frame from each UAV flight prior to the image's processing and Classification. The same vegetation survey is used for this study's training and validation data (50% used for training data and the remaining 50% used for validation).

Vegetation sampling involved recording the vegetation type in the field at each of the randomly generated points with the Emlid Reach Software application. A record of the Point Number and vegetation type was noted for each point. Once the Vegetation Survey was complete with every point having an allocated vegetation type the results were exported to ArcGIS Software. A polygon was created for each point representing the shape of the vegetation. This digitisation allowed the shape and texture elements of the training data to be used as supplementary information for OBIA.

While the UAV survey is capable of high-resolution mapping, there is a limit to its ability to identify plant species. Therefore, the minimum mapping unit of 10x10cm in size (twice the pixel resolution size) was employed in the vegetation sampling. The vegetation species was

not observed if it had a size less than 10x10cm or if in a single plot there was multiple vegetation species.

Pingao and spinifex sand binders are the most important species for dune establishment. However, the amount of pingao that was observed using the same random sampling as the mid to back dune study was less than 30. Nevertheless, due to the high ecological value of Pingao in Auckland Council's Terrestrial and Wetland Ecosystems Classification, key patches of Pingao were visually identified on a previous aerial image and recorded in the field.

Object-based Image Analysis (OBIA) uses pixel value and shape, compactness, texture, and spatial relationships. Therefore, training samples generation used a combination of fieldwork data and GIS-based manual digitising. This process involved locating the point at which the sample was collected and then manually tracing the outline of the plant. This allowed the OBIA to use this outline as additional information to the classification algorithm. Objects with two or more sample points within a single object were treated as a single sample. The shape outline could be used to train the image segmentation and assess the accuracy of the segmentation.

2.6 Data Exploration and Assigning Vegetation Classes

2.6.1 Classification of the vegetation

The number of categories in a classification scheme increases the likelihood of misclassification errors. A vegetation classification map will amalgamate vegetation species into various classifications for remote sensing projects. How the classification scheme is produced will depend on the project's aim, vegetation diversity and quality of the imagery and vegetation sampling. Therefore, great care needs to be taken when producing a

classification scheme. In this study, categories were created correlating to the goals of using UAVs for monitoring and dune rehabilitation.

Auckland council's classification scheme was used as a guide to identifying key vegetation species that should be targeted to assess dune health. Therefore, key invasive weeds such as tree lupin and pampas were given individual categories. Key native sand binders, pingao and Spinifex, which significantly impact dune morphology, were also given their categories. Other key native species characteristic of the DN2 classification scheme were also needed to be included as their own categories (Muehlenbeckia complexia, Phormium tenax and Ozothamnus leptophyllus). Ficinia nodosa and Carex Testacea were classified as a single classification of native sedges. All vegetation greater than 2 metres in height were classified as established following both dune succession zones literature and Auckland Council guidelines. Sand and exotic grass were also given individual categories as they represent a large proportion of the study site.

There were 12 classification classes assigned to the vegetation within the study area site. The classification schema can be seen in the below table, Table 4. The foredune comprises predominantly of sand/bareground, with sand binding species (Spinifex and Pingao) also present. The mid dune species consisted of flax, sedges, tauhinu, mulenbeckia, Lupin, pampas, herbland, bareground and dead vegetation. The back dune consisted primarily of Herbland and established forest (vegetation > 2m as per Auckland Council’s guideline employed in their dune field sampling).

Table 4: 12 Classification classes included in this study

Species	**Classification Class**	**Origin**
Spinifex sericeus	Spinifex	Native
Ficinia spiralis	Pingao	Native
Phormium tenax	Flax	Native
Ficinia nodosa and Carex Testacea	Sedges	Native
Ozothamnus leptophyllus	Tauhinu	Native
Muehlenbeckia complexa	Muelenbeckia	Native
Lupinus arboreus	Lupin	Exotic
Cortaderia selloana	Pampas	Exotic
Grassland and herbland	Herbland	Mixed
Mixed forest species	Established Forest (vegetation > 2m as per Auckland Council's guideline employed in their dune field sampling).	Mixed
Sand/bare ground	Bareground	N/A
Dead Vegetation	Dead Vegetation	N/A

2.6.2 Exploratory Data – Spectral Signatures

Comparing and contrasting histograms of spectral signatures of thematic classes is an essential step in understanding the effectiveness of classification algorithms. In many studies, differences between spectral signatures are used as the determining factor for thematic class choice. However, in this study, the goal was to isolate thematic classes of ecological importance (either native or exotic).

Therefore, the spectral signatures provide information of which classes are spectrally similar and have a greater chance of being misclassified. On the other hand, it also provided data on which classes were spectrally unique and should have high classification accuracy.

The spectral signatures were also compared between the two sample periods (November and March). The temporal comparison allows further data regarding times, both how the spectral signatures of an individual class changed over time and if the differences or similarities between different classes were enhanced or reduced.

2.7 Assigning Training Samples and Ground Truth Samples

In this study, both the training and validation vegetation samples were identified in the field and then manually digitised in ArcGIS Pro. The number and sampling technique used to acquire these sample types is crucial for the statistical rigour of the final accuracy assessment of the classification map.

Training samples were collected using a stratified random sampling methodology as previously mentioned in the field sampling section. However, the random stratified method used two thematic zones for sampling, not the twelve categories used for the Classification. Therefore, Van Genderen and Lock's (1977) equation of minimum reference samples was used to determine how many field sample plots should be used for validation. Van Genderen and Lock's equation for the selection of the minimum number of reference samples is as follows:

$$N = \frac{4(p)(q)}{E^2}$$

Where:

N = total number of points to be sampled

p = expected percent accuracy

q = 100 – p

E = allowable error

In Yeet al.'s (2018) review of object-based remote sensing studies, they found that reported accuracy ranged from as low as 42% to as high as 96%. The average accuracy assessment of the 209 reviewed articles was 85%. Using Van Genderen and Lock's equation, the minimum sample size of 20 samples per thematic category is required for an 85% classification accuracy. A minimum of 30 observations per class for a 90 percent accuracy (at 0.05 confidence level) was used for this study. From the previously conducted stratified random survey of dune succession zones, the thematic class with the least number of recorded samples was Pampas, with a total of 65 samples.

Therefore, a Python script was written to select 50 percent of samples from ESRI shapefiles randomly. The script was run on each thematic class individually to ensure the minimum number of samples per category was observed. This meant that the Pampas classification would have a minimum of 32 samples used as validation in the accuracy assessment.

2.8 Classification Schemes

In this analysis, both Pixel-based and OBIA Classification schemes were trialled. The three pixel-based classifications were: Maximum Likelihood Classification (MLC, Mahalanobis Distance and Neural Net. In addition, object-based Classification was performed in eCognition using the multiresolution segmentation algorithm and ruleset.

2.8.1 Pixel-Based Classifications

Supervised Maximum Likelihood Classification (MLC) is a classification scheme based on Bayes' Classification. The first step of the MLC is to calculate the mean and variance for each class (Shivakumar & Rajashekararadhya, 2017). It is based on the statistical likelihood of an individual pixel belonging to a particular class and assumes the mean and covariance follow a normal distribution (Richards et al.,1999). Furthermore, it uses a maximum a posteriori estimation (MAP), a principle that is used to create a point estimate based on data following regular normal distribution (Jensen., 2000). MLC was carried out in the ENVI 5.3 software.

Mahalanobis Distance Classification is a distance-based classifier. It uses all the statistics of each class; however, unlike MLC, it assumes all covariances are equal and, therefore, a faster algorithm to perform (Richards & Richards, 1999). Also, similar to MLC, it assumes a normal (Gaussian) distribution.

The final pixel-based classification scheme was the Neural Net Classification, also performed in the ENVI software. The Neural net classification in ENVI is a form of Artificial Neural Network (ANN) that follows a standard back-propagation methodology using supervised machine learning (*Exelis Visual Information Solutions, 2010)*. Neural networks use a series of nodes and layers to predict an output, such as a classification type (Maxwell et al., 2018). Neural Networks are data-driven and adapt after multiple runs or iterations in which a pixel will be 0 (not within a class) or 1 (within a class) (Zhang & Chang, 2015). Neural Net Classification follows a back-propagation loop whereby each iteration builds upon the previous loop creating a positive feedback loop. Each iteration adds additional data used to determine the final output result. In this study, a total of 1,000 iterations were carried out for each analysis.

2.8.2 Object-Based Classification

Object Based Image Analysis (OBIA) was performed in eCognition 9.3 software. eCognition is a software tool used for OBIA that is very powerful because the Objects are created using multiresolution segmentation. OBIA includes an additional step before the analysis of the pixels, image segmentation. Image Segmentation creates groups of pixels with similar shared attributes known as objects. Attributes including size, distance, spectral similarity, and form determine similarity and are the criterion for creating objects with shared/similar attributes (Baatz et al., 2000). The similarity criterion is run on different scales simultaneously; therefore, the same multiresolution segmentation algorithm can be used for any number of different scales depending on the objective. Scale Parameter (i.e the size of the objects created), Shape/Colour weighting (i.e. defining whether the shape of an object or colour/reflectance value, will have greater influence) and object compactness are the three user controlled variables within the multiresolution segmentation algorithm (eCognition Developer Trimble, 2014).

Scale Parameter defines the size of the objects created. It is dependent on the objectives of the data and the data itself. Therefore, multiple trial and error tests are required in the preliminary analysis (Kim et al., 2009). The researcher needs to be balance any loss of micro-scale data from a scale parameter too large and weigh this against creating a scale parameter that is too small, which results in the target classification class of interest being split into many different objects instead of a single output. As part of the preliminary analysis attempting to define the scale parameter for this study, Estimation of Scale Parameter (ESP) was performed on the images.

ESP generates image objects at multiple scales using a bottom-up approach, i.e. starting with a small-scale parameter and increasing iteratively while also calculating the Local Variance (LV) at each scale parameter (Dragut et al., 2010). LV is defined as the heterogeneity of

colour and shape that is observed at each scale. Therefore, allowing a researcher to quickly determine which scale parameter is best suited for the given application (Dargut et al., 2010).

Peaks in LV graphs in relation to the Rate of Change (the blue line in Figure 9) usually indicate the point at which the data can be segmented appropriately. However, this study aimed to create a reusable set of rules for direct comparison with the pixel-based classifications. Therefore, a single scale parameter of 30 (which had a local variance of 0.9 was decided to be run over the whole image), see Figures 10 and 11.

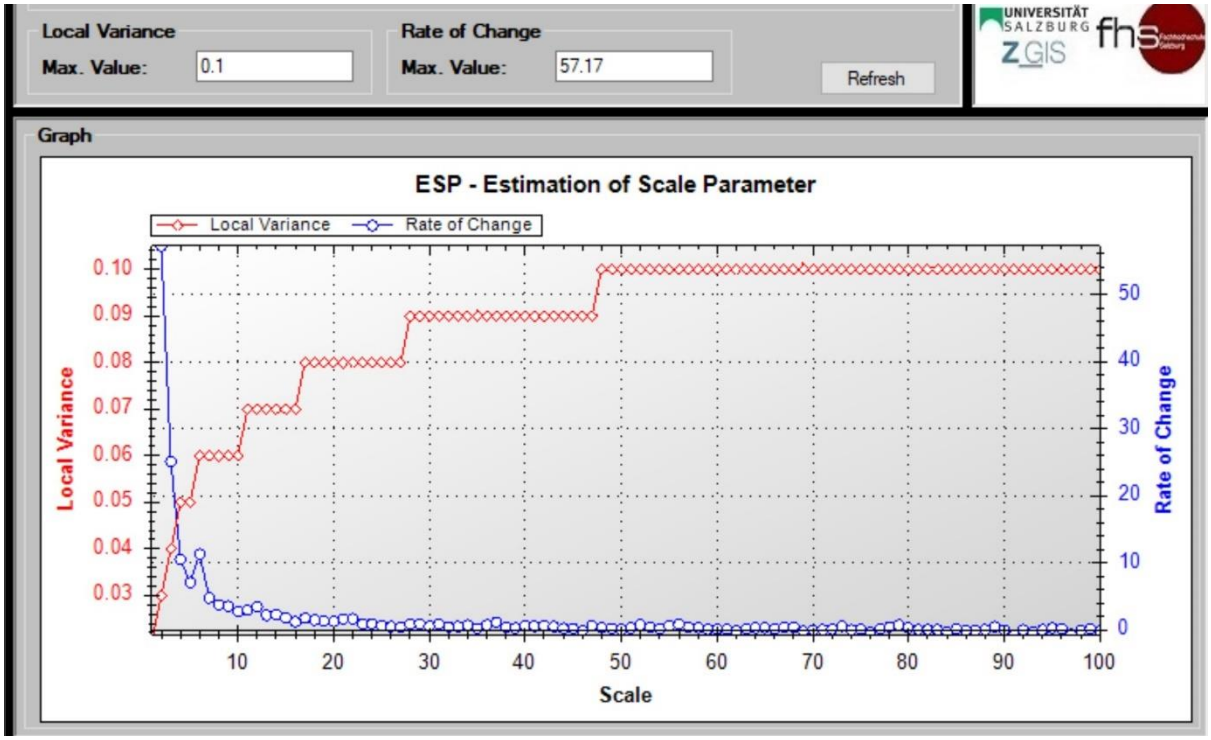

Figure 9: Graph of Estimation of Scale Parameter (ESP) local Variance and Rate of Change.

Another option would be to create multiple different scale parameters for different classes i.e. a large scale parameter for back dune vegetation and a small scale parameter for pingao. This could be explored in future studies. An example of the output of the scale factor of 30 can be seen in Figure 9.

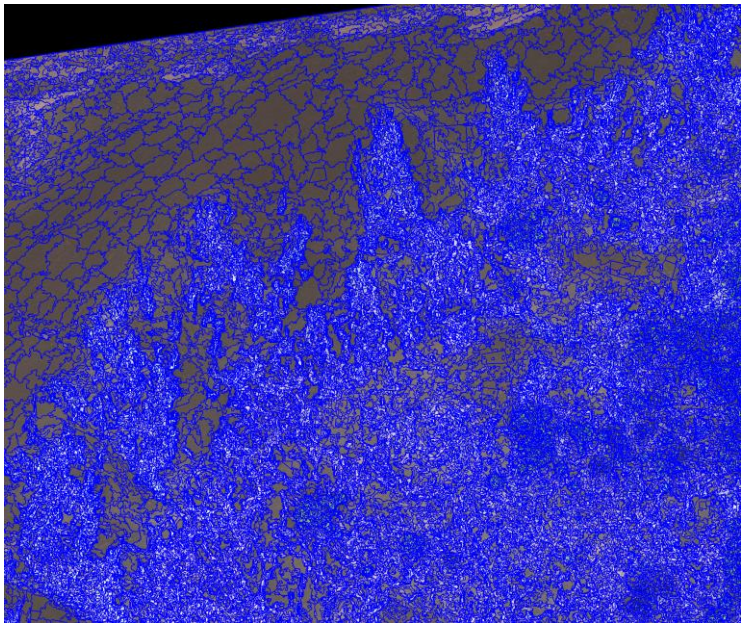

Figure 10: Scale Parameter 30 output within eCognition Software

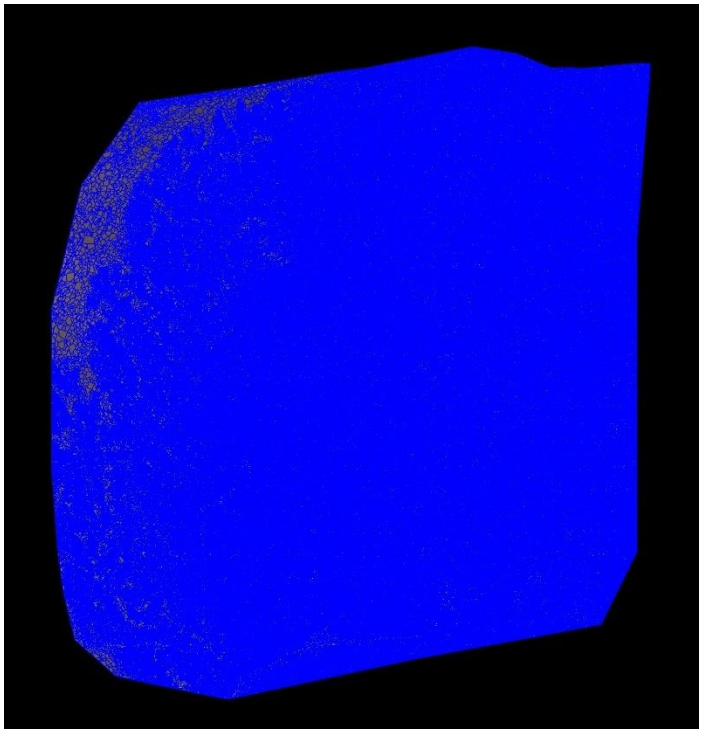

Figure 11: An example of the image objects created at Scale Parameter 30 for the whole of Karekare Beach

As mentioned earlier, there are three user-determined parameters within the multiresolution segmentation algorithm. The other two parameters are required to be changed. The first is the Shape ratio (0.0 shape has no influence on objects and is solely driven by the colour of the image layer to 1.0 determined exclusively by colour). The other is compactness which determines how compact the objects will be. Determining these two values involved a series of trial-and-error tests where the image layer underneath the objects was examined to determine whether the objects matched the real-life vegetation classes of the image, see Figure 12.

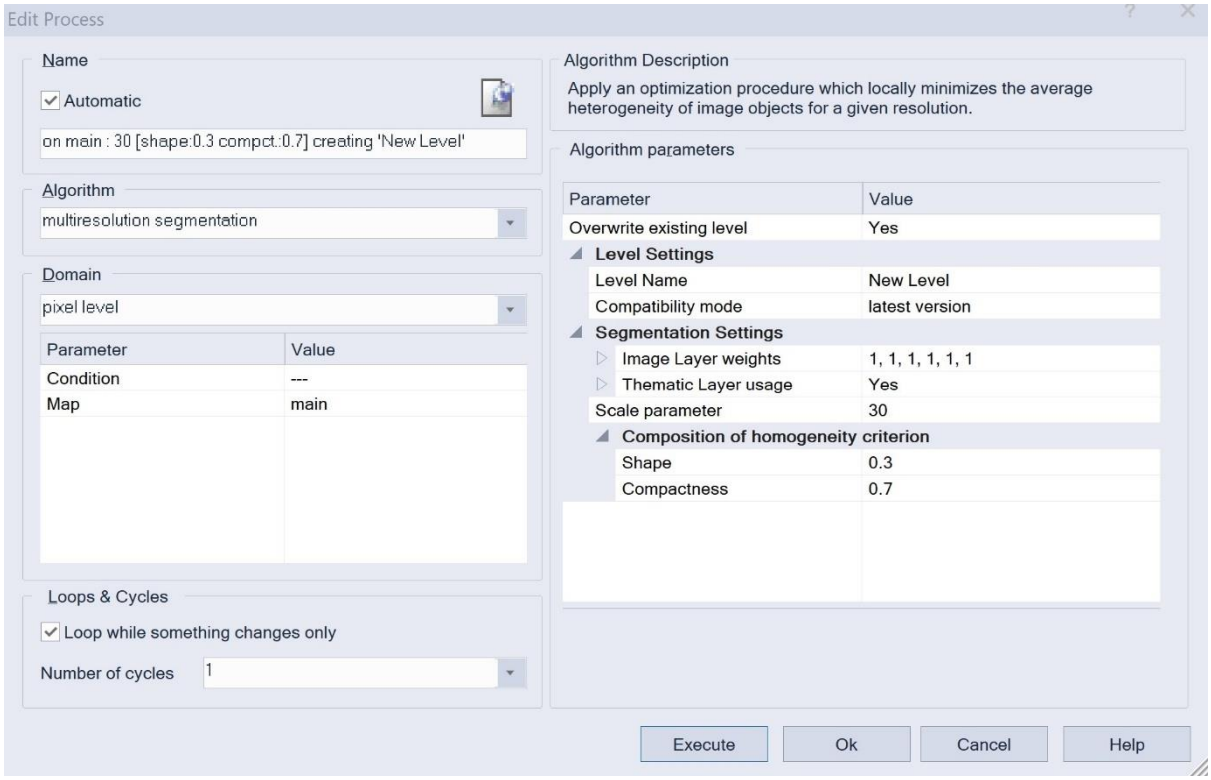

Figure 12: Variables used within the eCognition Software for multiresolution segmentation.

Once the segmentation was complete, the next stage in the analysis was to create training samples for the classification algorithm within eCognition. The same shapefiles from the pixel-based classifications were used to create samples for the OBIA classification.

Classification analysis could occur once the samples were made and assigned to their vegetation classes (see Figure 13)

Figure 13: The 12 Classifications used - consistent with both the OBIA and pixel-based analysis

The next step in the OBIA process tree was to create samples to attribute features of the sample set used for the Classification. Multiple different features can be included as data for the algorithm with eCognition. Choosing the correct features will depend on the study. It is unfeasible to select all features and run the algorithm, especially on a data set such as the one on Karekare beach, where 100s of thousands of objects were created for a single image. Therefore, key object features representative of the vegetation classes were chosen. These included: Mean and standard deviation values for all bands, compactness and roundness of the objects, and texture values, including standard deviation of texture values after the Haralick method, which looks at textural variance and orientation (Figure 14 and 15)

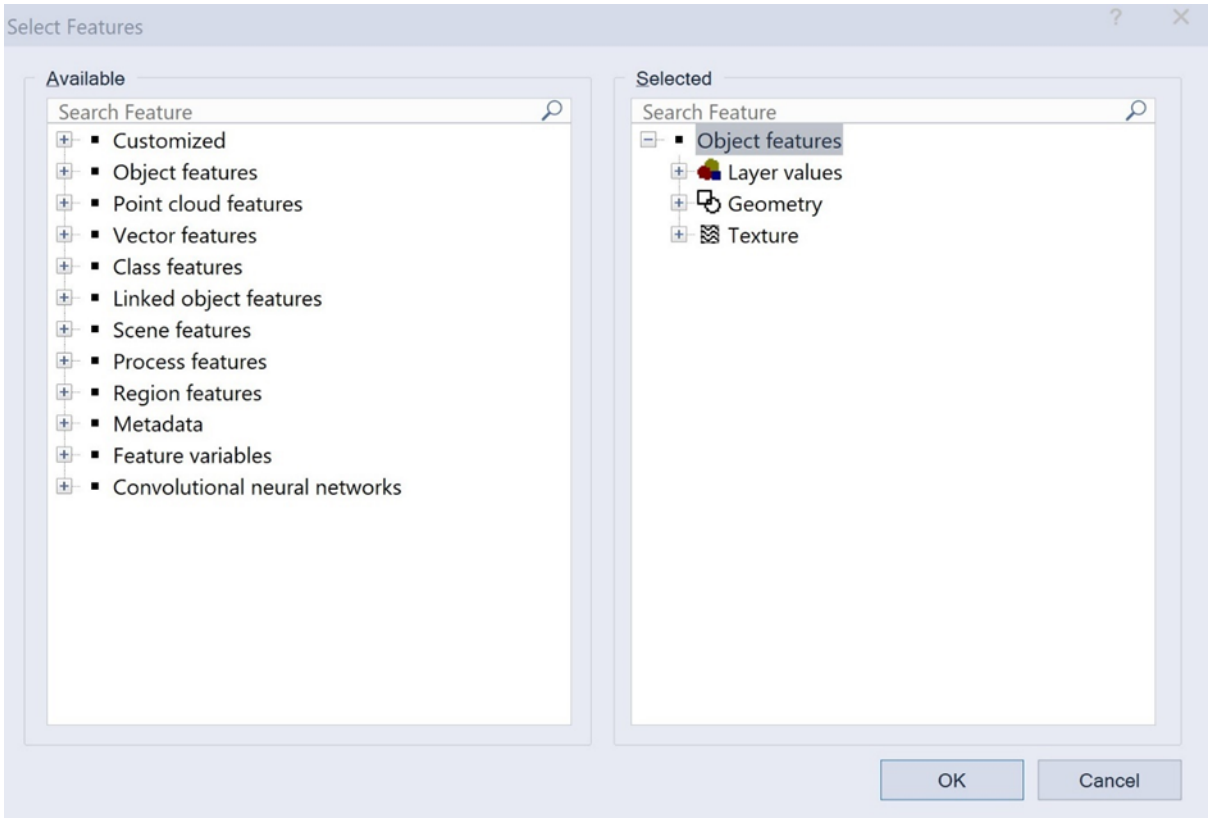

Figure 14: Selectable Features available to be included as reference data for classification samples.

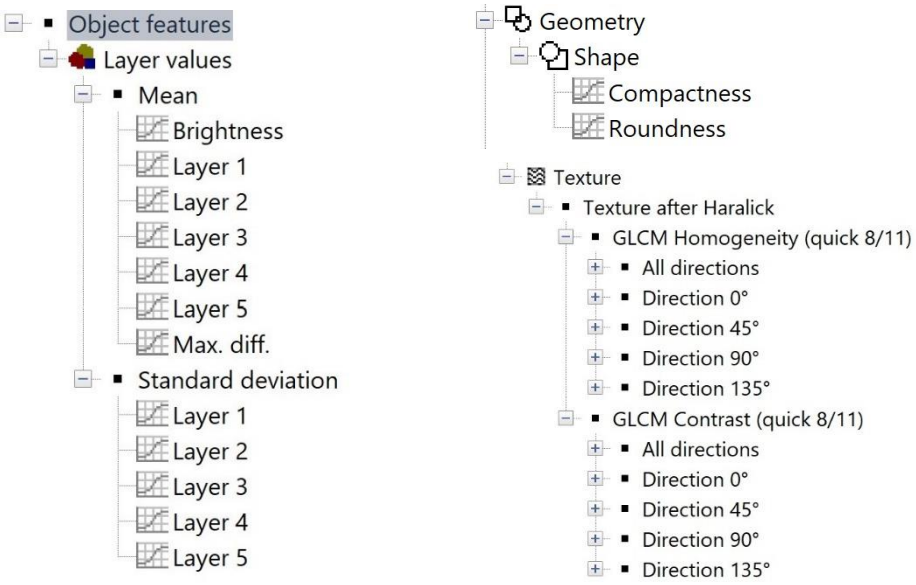

Figure 15: Object Feature variables selected to train the multiresolution segmentation in eCognition.

Once the samples had been populated with data resulting in their attributes, Classification could be carried out on the complete image. Like the pixel-based methods, the training sample data is used to extrapolate and classify all objects that are not currently assigned a class as a training sample object. The result of this process is the final classification map, and the last step is to export the data to a shapefile in order to carry out an Accuracy Assessment. Refer to Figure 16 for an overview of the complete Process Tree used for OBIA analysis. The same Process Tree was used for all of the different classification schemes, although the training samples for November and March were changed to reflect the sampling that was carried out at the two different time periods.

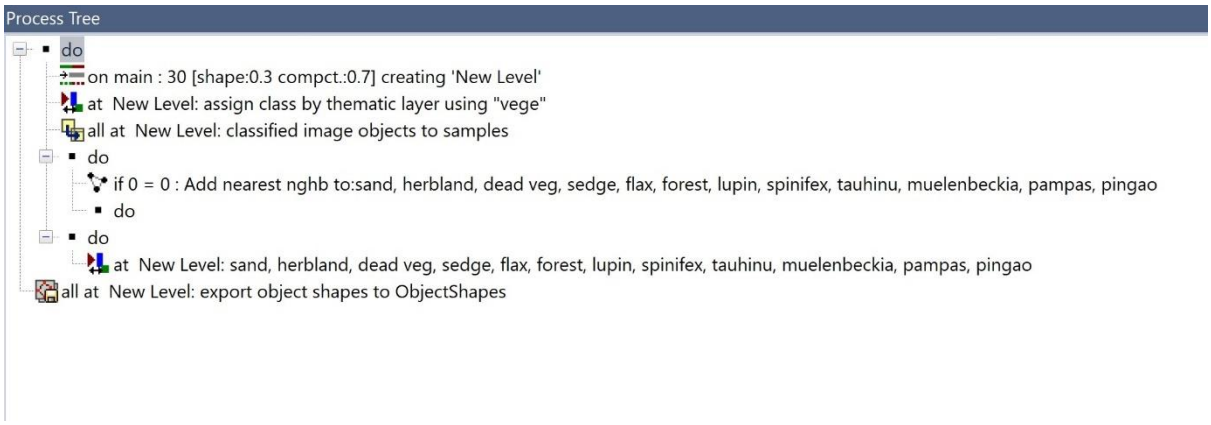

Figure 16: Process tree for OBIA within eCognition

2.9 Accuracy Assessment

The accuracy assessment methodology was consistent for all the classification outputs. The polygons excluded from the initial Classification (50% of the total) were now the ground truth data to assess accuracy. The accuracy assessment involved creating a methodology to determine whether the output classification Thematic class pixels matched the Thematic class of the ground control pixels. The individual polygons created from the OBIA analysis were

of varying size. Therefore, the polygons were segmented into pixel-sized objects using the fishnet tool in ArcGIS to create a representative assessment and for accurate comparison with the pixel-based methods.

An Intersect with the outputs of the different classification methods and the ground truth data was carried. Once the intersect was completed, the class names of the output and ground truth pixels needed to be kept consistent. A new field in the attribute table was created to match the Vegetation type of the ground truth data with the various output classifications (vege must match Class_1). The attribute table was then exported as a text file.

The next step involved using R code to create a confusion matrix for each classification method. The caret statistical package was imported into R Studio. A script was produced to create a confusion matrix from the export attribute tables of the classification outputs (see Figure 17).

```
library(caret)

d2 <- read.table("march_VI_ecog.txt", sep = ",", header = TRUE)
d2

expected <- factor(d2$vege)
predicted <-(d2$Class_1)

expected
predicted

results <- confusionMatrix(data=expected, reference=predicted)
print(results)
```

Figure 17: R code of Confusion Matrix created for Accuracy Assessment of all pixel-based and OBIA classifications

3. Results

3.1 Chapter Layout

This chapter presents outcomes of the image processing and classification workflows aimed at addressing the two thesis objectives. In the first part of this chapter, results are related to the evaluation of the spectral signature profiles for the different dominant vegetation types across the Karekare sand dune ecosystem for two seasons. Spectral signature profiles are presented as histograms that indicate the distribution of reflectance values for different vegetation types in terms of three key multi-spectral wavelength bands (Red, Near Infrared, and Red Edge) and derived spectral indices (NDVI, Ratio etc., see 3.3.1)When looking at histograms, the ideal situation would be to have the histograms of each vegetation type having distinctly different spectral reflection profiles, and peak reflectance values, for each data band, with minimal overlap. This is rarely the case, and so the spectral profiles provide initial useful insights into how well we might expect a vegetation type to ultimately be well-classified relative to other types, and whether this might differ depending on the season of imagery collection. In the second part of the chapter, different vegetation classification methods are compared in terms of the accuracy with which vegetation types are discriminated across the sand dune vegetation complex.

3.2 Examination of Spectral Reflectance Profiles for Different Vegetation Types

3.2.1 Training and Ground Truth Data acquired from Vegetation Survey and manual digitisation

The training data samples were used to generate spectral profiles for each vegetation class. A summary of the number of pixels created for the November and March Vegetation samples are shown in the following Tables 6 and 7. There is slight variance in the number of pixels

created for each class between November and December. This variance is accounted for by the vegetation changing in size between the two seasons.

Table 5: Number of Pixels used for each class for Ground Truth and Training Data in November

Class	Training Sample Pixels	Ground Truth Pixels	Total number of Pixels from the Vegetation Survey
Spinifex	7388	7388	14776
Pingao	831	831	1662
Flax	27224	27224	54448
Sedges	39911	39911	79822
Tauhinu	38750	38750	77500
Muelenbeckia	30317	30317	60634
Lupin	102288	102288	204576
Pampas	2414	2414	4828
Herbland	43545	43545	87090
Established Forest	136550	136550	273100
Bareground	25648	25648	51296
Dead Vegetation	6375	6375	12750
Total	461241	461241	922482

Table 6: Number of Pixels used for each class for Ground Truth and Training Data in March

Class	Training Sample Pixels	Ground Truth Pixels	Total number of Pixels from the Vegetation Survey
Spinifex	10497	10497	20994
Pingao	2567	2567	5134
Flax	45957	45957	91914
Sedges	39698	39698	79396
Tauhinu	34545	34545	69090
Muelenbeckia	55572	55572	111144
Lupin	47907	47907	95814
Pampas	22408	22408	44816
Herbland	27229	27229	54458
Established Forest	97882	97882	195764
Bareground	22716	22716	45432
Dead Vegetation	19202	19202	38404
Total	426180	426180	852360

3.2.2 Red, near-infrared, and red edge histograms across all vegetation classes

Given that vegetation types can usually be best discriminated based on how they differentially absorb red light, or reflect near-infrared light, the Near-infrared and Red Histograms are very important to the overall spectral profile of a vegetation class. These profiles can provide critical insights into different levels of ‘greenness’ of the different

vegetation types and how this might impact on spectral responses and, ultimately, the ability to classify them.

Spectral profiles across the 12 vegetation types for red band reflectance (Figure 18) show that distinct bell curves characterise some vegetation profiles for both months. However, there is a shift in the profiles between November and March. For both months, many vegetation classes overlap and have similar spectral signatures, including the Muelenbeckia and Tauhinu classes or the Lupin and Flax classes that share very similar spectral signatures

Red Band Reflectance Values

The red band reflectance values of the vegetation for the March imagery, in comparison to the November imagery, were very low, with most of the pixels recording reflectance values below 0.08. Because the reflectance values were low, more classes had similar histograms with overlapping reflectance values.

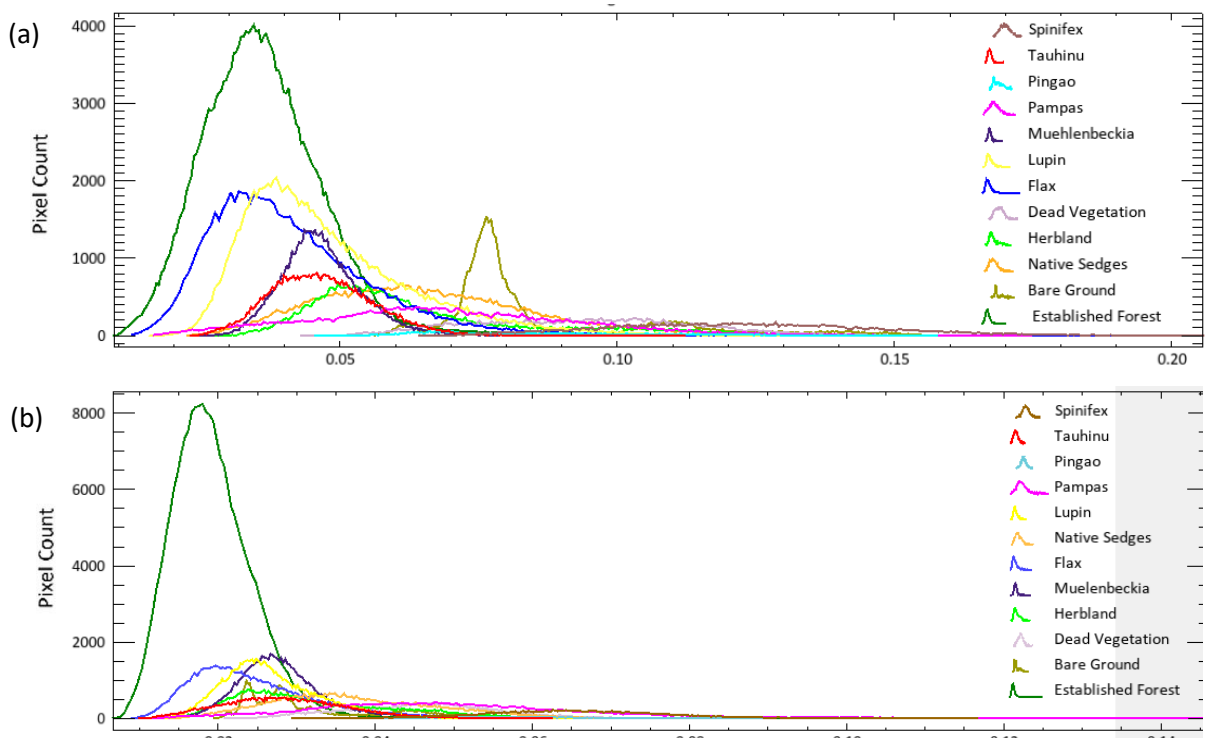

Figure 18: Band 3 -Red (661 to 675 nm wavelength) spectral reflectance profile histograms created for the 12 vegetation classes identified at the Karekare Beach sand dune site, for (a) November imagery and (b) March imagery.

Near InfraRed Reflectance Values

November: Near InfraRed (Band 4) has a wavelength of 842 nm centre with a 57 nm bandwidth. The histograms here look very different from the ones seen in band number three. In particular, the Tauhinu class is now separated from the Muelenbeckia class. Therefore, these spectral differences could aid in the classification algorithm generation. Lupin also seems to have a slightly displaced curve compared to the flax classification seen earlier. However, other classes such as Muelenbeckia and Flax have very similar spectral curves within this wavelength.

March: Band 4 (Near-Infrared) also shows much lower reflectance values than in November, with maximum values close to 0.4 instead of 0.8 in November. However, the bell curves were less clustered together because plants have much higher reflectance values in the near-infraRed and Red-Edge wavelengths. In particular, the Bare Ground class had a very distinctive low reflectance value for this spectral band. Native Sedges, Tauhinu and Dead Vegetation all had distinct histogram curves. However, there was a lot of overlap within most of the classes, including Established Forest, Muelenbeckia, Flax, Herbland and Pampas.

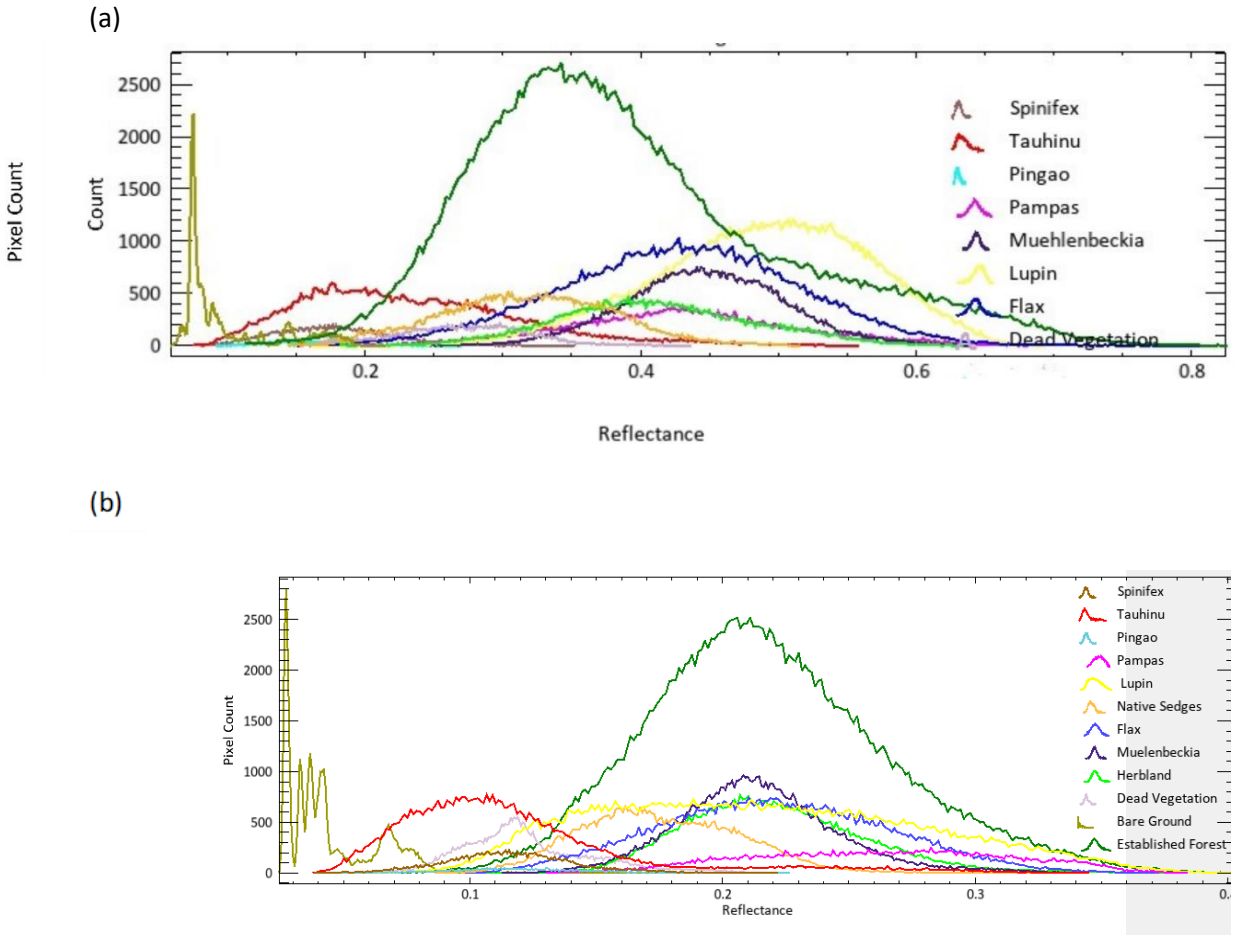

Figure 19: Band 4 Near Infrared 842 nm centre with a 57 nm bandwidth a) November Imagery b) March Imagery

Red Edge Reflectance Values

November: Figure 20a shows the spectral signatures of the twelve thematic classes within the RedEdge band wavelength (717 nm centre, 12 nm bandwidth). The Lupin class has lower reflectance values than Muelenbeckia, whereas the inverse was true for the Near InfraRed histogram. However, Herbland and Established Forest share similar curves in the Near InfraRed and RedEdge bands. There is more significant differentiation in the Red band histogram in Figure 18 for these two classes. These basic statistics of the different classifications represented in visual graphics are crucial for Remote Sensing. It can inform which classifications will be more likely to be classified correctly. It will be a key indicator for the results and the final classification accuracies and errors.

March: As seen with the November survey, the RedEdge spectral band provided subtle differences compared to the RedEdge band and was a valuable addition for this study (Figure 20b). In particular similar to the November study, Flax and Muelenbeckia showed more significant differentiation between the two classes. However, many of the classes fall within the 0.05 and 0.15 reflectance ranges, which shows how difficult characterising different vegetation classes based on spectral data can be.

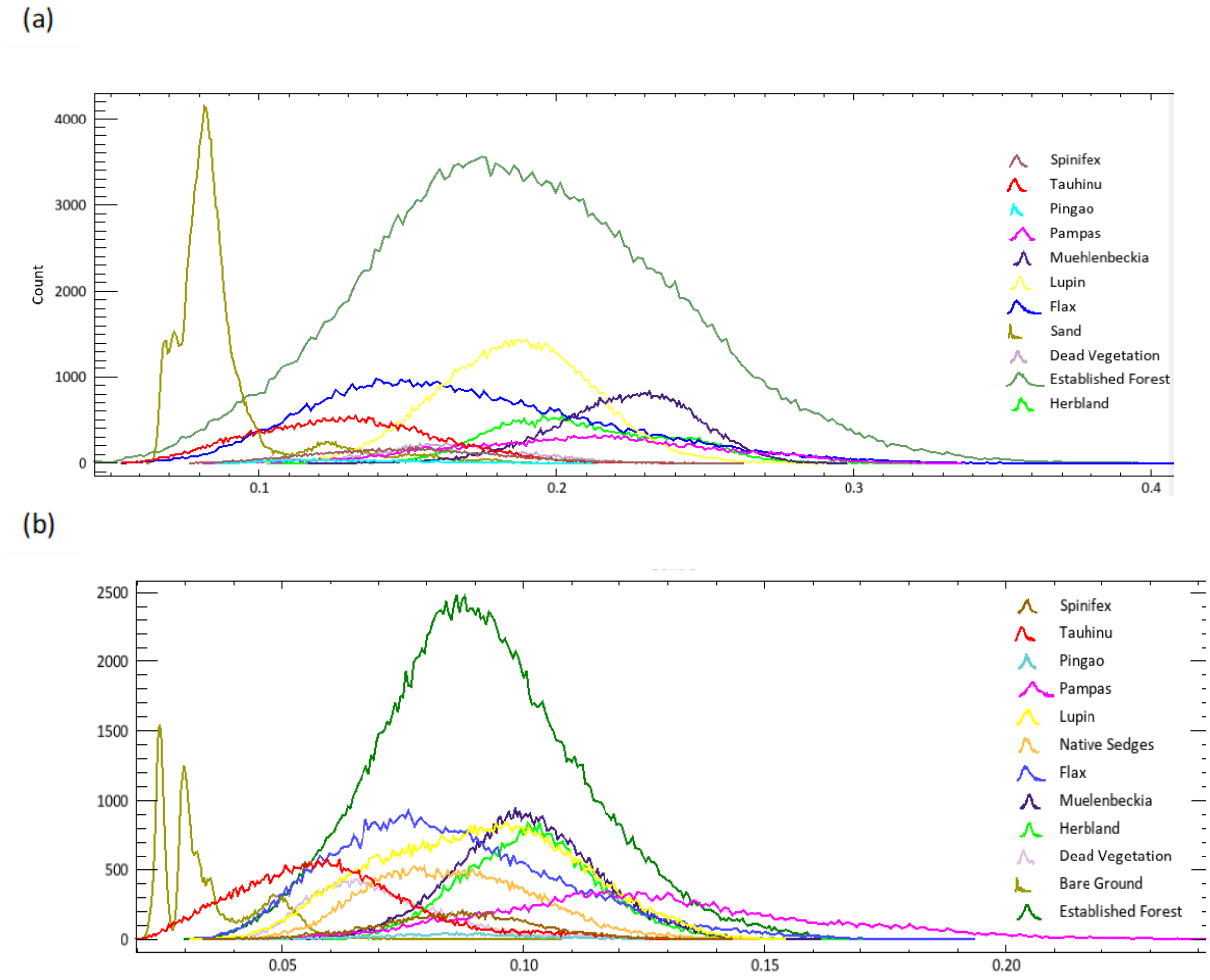

Figure 20: Band 5 (RedEdge) All Vegetation Classes a) November and b) March

3.2.3 Spectral signature comparisons

A few thematic classes had similar spectral profiles, which increases the probability of misclassification. However, some classes were of high value to differentiate. For example, the differences between Muelenbeckia and Pampas. One is a native species (Muelenbeckia) while the other is an exotic species. Therefore, it was necessary to differentiate between these classes even though they had similar spectral profiles. The following section indicates the different classes that have similar spectral profiles and therefore have a greater probability of misclassification.

November Spectral Signature Analysis

Forest and Herbland

Figure 21 shows the difference between Established Forest and Herbland using the Normalised Difference Vegetation Index (NDVI). While the pixel count is different, the overall curve is very similar. If this data was used exclusively, it would result in an inferior classification result. However, there were slight differences in the histogram shapes in band three red. Therefore, it was hoped that there would be enough differentiation within the classes for an accurate result. The Established Forest and Herbland also have very different textural qualities. Therefore, it would be expected that the object-based analysis would produce higher quality results than the pixel-based algorithms.

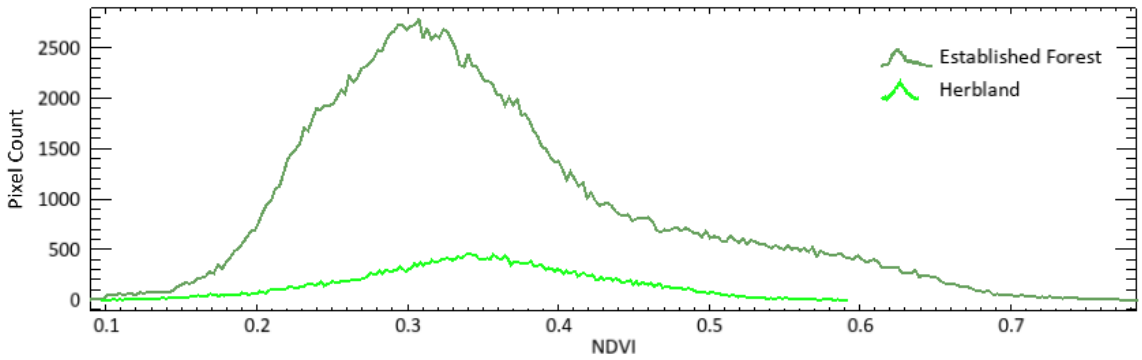

Figure 21: Established Forest and Herbland NDVI histograms for the November Imagery

Lupin and Flax

Lupin and Flax near-infrared values have a slight overlap; however, the overall curves are very different (see Figure 22). Lupin has a more Normally Distributed curve, whereas Flax has a skewed curve. It is an important factor to consider that all of the classification algorithms assume normally distributed data. Therefore, the flax class could show results that are not expected.

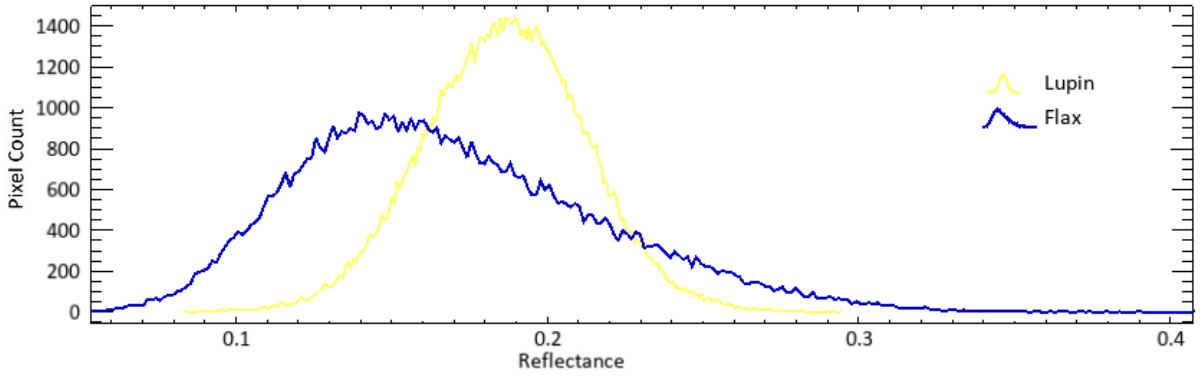

Figure 22: Lupin and Flax Near Infrared values for November Imagery

Pingao and Pampas

An example of two classes that will be very unlikely to be misclassified is Pingao and Pampas. Figure 23 shows two distinct curves with minimal overlap in the infrared band. Judging from this histogram, the classification accuracy would be very high if the algorithms were to be run, focusing only on these two classes.

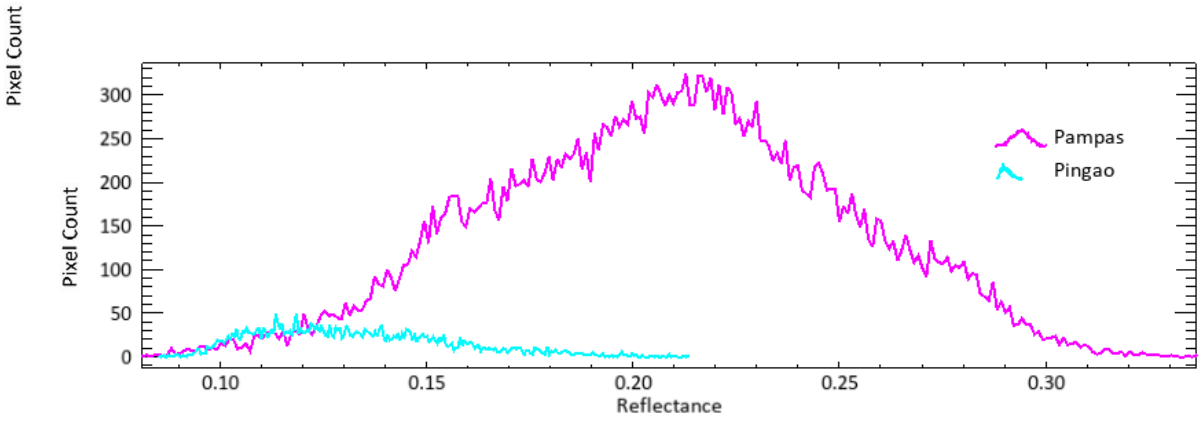

Figure 23: Pingao and Pampas Near Infrared values

March Spectral Signature Analysis

Like the November analysis, both Forest and Herbland had very similar NDVI values, and it would be challenging to differentiate these classes, see Figure 24. Muelenbeckia and Herbland show almost identical curves in the RedEdge band; however, there were slight differences in the NDVI vegetation index (Figure 25). It will be interesting to observe these two classes' different commission and omission errors for the 5-band classifications compared to the 15-band algorithms with the vegetation indices included.

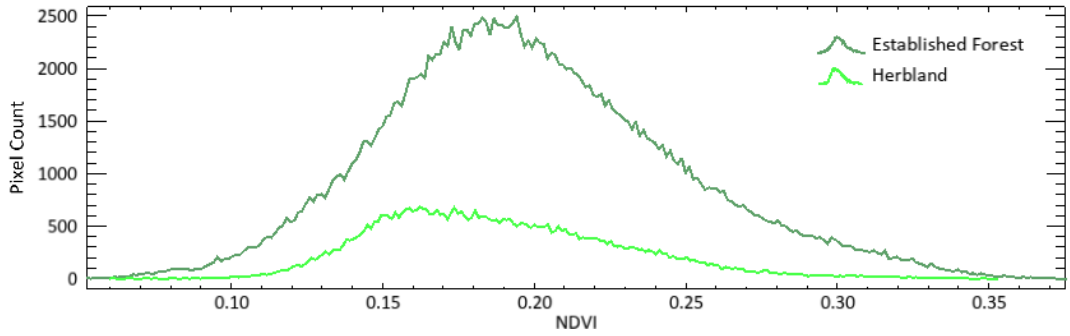

Figure 24: Established Forest and Herbland NDVI histograms

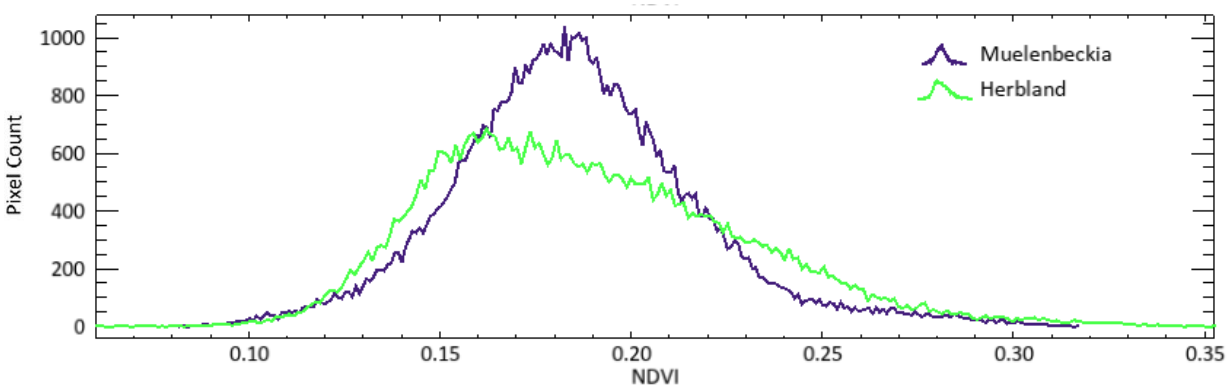

Figure 25: Muelenbeckia and Herbland NDVI Histograms

3.2.6 Temporal Variation in Spectral Signatures

There was a lot of difference between the output histograms of the November and March surveys. For example, Figure 26 shows the difference in NDVI between March and November for tree lupin (Lupin class); the NDVI values are approximately four to five times lower for this class in March compared to November. This was evident while on-site also as in November the Lupin was in flower and green; however, in March, the Lupin was not in bloom, and many of the green leaves had also fallen off. Tauhinu also showed a similar reduction in NDVI reflectance values in March compared to November (Figure 27). In both cases, the spectral signatures of the respective classes are entirely different between November and March.

Lupin November vs March NDVI variations

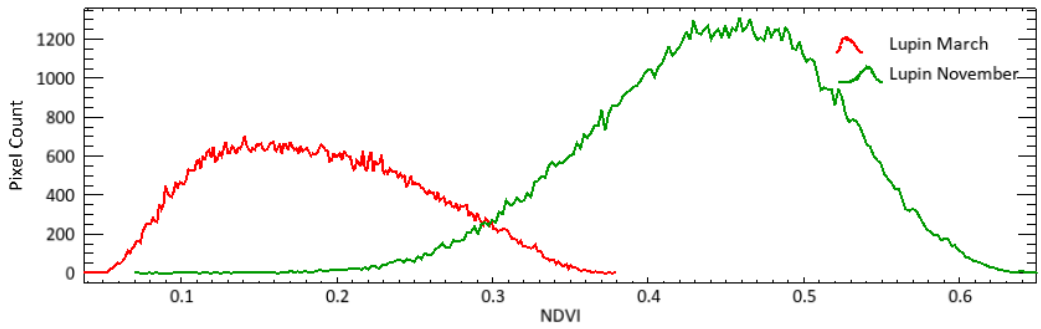

Figure 26: NDVI values for Lupin in March and November

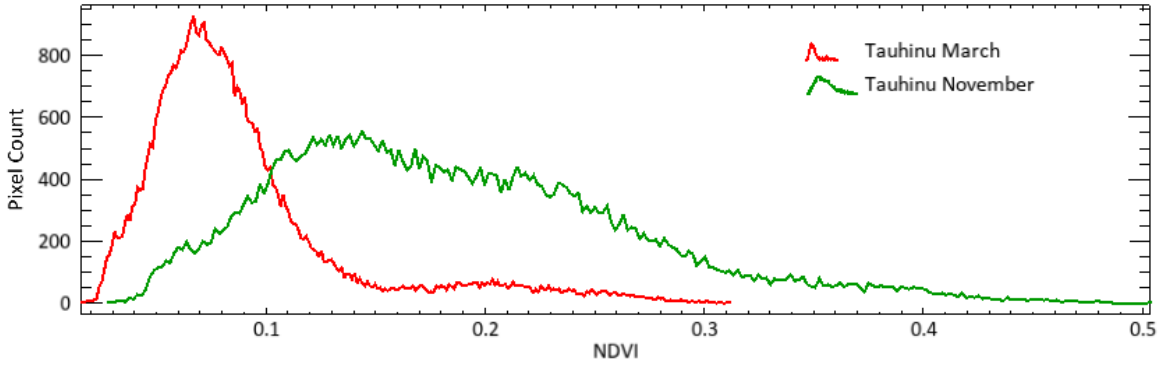

Figure 27: NDVI values for Tauhinu in March and November

Two classes that showed very similar NDVI values for both the November and March studies were Pingao and Spinifex (Figures 28 and 29). Both had a relatively low NDVI value, and because they are both foredune species, they are more resilient to drought conditions. This exemplifies how different vegetation species will have dramatically varied responses to seasonal variability and moisture availability. The difference is striking, especially when the two results are compared to the graphs of Lupin and Tauhinu NDVI values which show significant seasonal variability.

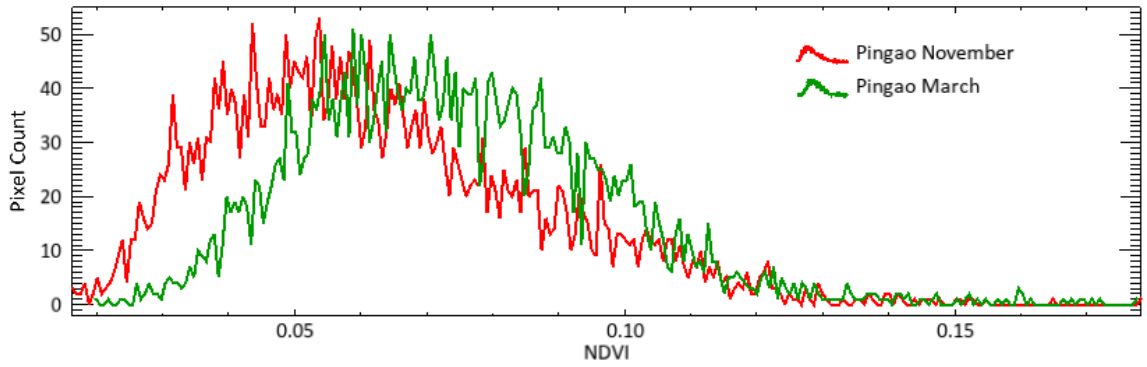

Figure 28: NDVI values for Pingao in March and November

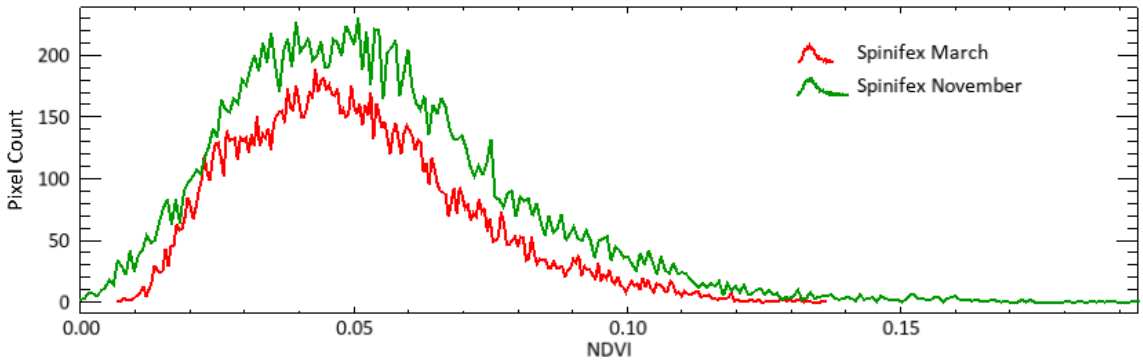

Figure 29: NDVI values for Spinifex in March and November

3.3 Image Classification of Vegetation Types on Karekare Beach Sand Dunes

3.3.1 Pixel-Based Results

In this section, confusion matrices will be created for all the different pixel-based classification algorithms. These include Maximum Likelihood, Mahalanobis Distance and Neural Net. There will be two confusion matrices generated for each survey (March and November). The two confusion matrices will consist of one using only the five spectral and one using the five spectral bands, and the other ten vegetation indices.

Pixel-Based Confusion Matrices

Maximum Likelihood

November Maximum Likelihood no Vegetation Indices

Overall Accuracy = 74.00%

Kappa Coefficient = 0.7017

The first results to be analysed are the Maximum Likelihood values. The overall accuracies with no vegetation indices were 74.00%. Overall, these results are very similar. Some vegetation classes had very high producer accuracies, including Spinifex (98.15%), Pingao (95.01%), Muelenbeckia 89.86% and Bare ground (98.72%). However, there were many examples where the accuracy was very low and below 50% accuracy in some cases. For instance, Pampas has an accuracy of 44.32%, and Herbland had an accuracy of 50.37%. Interestingly both of these were misclassified not by one but multiple different classes. Pampas was misclassified as Herbland 18.8% of the time, Flax 10.69 and Muelenbeckia 8.49%.

Table 7: November Maximum Likelihood no Vegetation Indices

	Tauhinu	Spinifex	Sedges	Pingao	Pampas	Muelenbeckia	Lupin	Herbland	Flax	Dead Vegetation	Bareground	Established Forest	Row Totals	Reliability(%)
Unclassified	0	0	0	0	0	0	0	0	0	0	0	0	0	
Tauhinu	30674	0	252	17	395	57	1393	83	532	0	1	4129	37535	81.72
Spinifex	198	9000	0	70	0	0	9	2	0	0	244	0	9524	94.50
Sedges	294	0	26405	0	1464	912	511	1135	3797	1869	0	482	36870	71.62
Pingao	1034	82	0	1951	0	0	0	0	0	0	0	0	3067	63.61
Pampas	99	0	708	6	9717	222	1916	1231	3038	69	0	768	17774	54.67
Muelenbeckia	339	0	1549	0	1862	44772	195	1829	1142	34	0	12754	64476	69.44
Lupin	602	0	91	0	1461	5	62494	1004	5758	0	0	4272	75686	82.57
Herbland	750	12	835	8	4122	1491	1659	7805	1990	96	0	13991	32760	23.82
Flax	400	0	2265	0	2344	350	8591	1236	37535	0	0	1916	54636	68.70
Dead Vegetation	150	23	8880	0	531	252	27	876	21	37535	36	684	49016	76.58
Bareground	3	52	0	0	0	0	0	0	0	0	21610	0	21665	99.74
Established Forest	2079	0	114	1	28	1765	1558	293	586	0	0	81980	88404	92.73
Column Totals	36622	9170	41099	2053	21923	49826	78353	15494	54399	39603	21891	120976	491411	
Cover Type Accuracy (%)	83.76	98.15	64.25	95.01	44.32	89.86	79.76	50.37	69.00	94.78	98.72	67.77		

November Maximum Likelihood with Vegetation Indices

Overall Accuracy = 74.50%

Kappa Coefficient = 0.7063

The results, including the vegetation indices, were very similar to the results without the vegetation indices. The overall accuracy was 74.50% compared to 74.00%. The same classes as the previous confusion matrices had very high accuracy percentages: Spinifex 97.82%, Pingao 94.72% Muelenbeckia 90.23% and Bare ground 98.62%. Herbland had a decreased accuracy of 41.93%, while Sedgeland decreased from 64.25 to 60.58%. Pampas had an even lower accuracy of 37.29 and was confused with Herbland 26.04% of the time. Overall the results between using the 5-band sensor and the 15-band stack were very similar.

Table 8: November Maximum Likelihood with Vegetation Indices

	Bareground	Dead Vegetation	Flax	Established Forest	Herbland	Lupin	Muelenbeckia	Pampas	Pingao	Spinifex	Tauhinu	Sedges	Row Totals	Reliability(%)
Unclassified	0	0	0	0	0	0	0	0	0	0	0	0	0	
Bareground	21765	0	0	0	0	0	0	0	0	49	2	0	21815	99.77
Dead Vegetation	39	7454	17	493	716	49	271	557	4	39	179	9415	19232	38.76
Flax	0	0	38798	2010	1050	8516	436	2227	0	0	603	3131	56773	68.34
Established Forest	0	1	571	84922	954	1122	2301	58	0	0	2108	104	92140	92.17
Herbland	0	68	2326	2064	6568	2640	872	5772	0	37	771	1106	22224	29.56
Lupin	0	0	7187	4369	1056	64434	8	1772	0	0	1109	106	80041	80.50
Muelenbeckia	0	13	1529	18104	2387	300	45453	1845	0	0	531	1855	72017	63.11
Pampas	0	36	1887	441	1728	846	14	8265	4	9	19	457	13706	60.30
Pingao	0	0	0	0	0	2	0	0	1966	69	1425	0	3462	56.79
Spinifex	261	0	0	0	0	31	0	0	72	9069	93	0	9527	95.19
Tauhinu	4	0	320	4197	19	916	18	149	24	0	29819	205	35672	83.59
Sedges	0	2042	2362	701	1186	358	999	1517	5	0	365	25172	34708	72.53
Column Totals	22068	9614	54997	117300	15665	79214	50374	22164	2076	9271	37024	41551	461317	
Cover Type Accuracy (%)	98.62	77.53	70.55	72.40	41.93	81.34	90.23	37.29	94.72	97.82	80.54	60.58		

March Maximum Likelihood no Vegetation Indices

Overall Accuracy = 75.70%

Kappa Coefficient = 0.7208

The March maximum likelihood confusion matrices will be analysed next. The March analysis's overall accuracy without vegetation indices was slightly higher than the November classification (overall accuracy: 75.70%). Bareground (96.76%), Spinifex (95.12%), Pingao (90.34%) and Muelenbeckia (85.52%) again had high classification accuracies. However, in

March, Pampas was classified much more accurately 62.95% an 18.63% increase from the November analysis using five spectral bands. Herbland was also classified with greater accuracy (65.61% compared to 50.37%).

Table 9: March Maximum Likelihood no Vegetation Indices

maxlik5														
	Bareground	Dead Vegetation	Flax	Established Forest	Herbland	Lupin	Muelenbeckia	Pampas	Pingao	Spinifex	Tauhinu	Sedges	Row Totals	Reliability(%)
Unclassified	0	0	0	0	0	0	0	0	0	0	0	0	0	
Bareground	22423	0	0	0	0	0	0	0	1	213	79	0	22716	98.71
Dead Vegetation	170	8856	184	211	16	2319	116	206	7	58	1053	6006	19202	46.12
Flax	0	4	35640	5375	835	282	134	2177	10	0	6	1494	45957	77.55
Established Forest	0	104	1452	88860	525	3549	2778	142	0	0	215	257	97882	90.78
Herbland	7	300	6176	5115	9809	1601	1214	1928	9	0	49	1021	27229	36.02
Lupin	3	184	1165	3809	62	38855	720	765	3	23	922	1396	47907	81.11
Muelenbeckia	0	317	315	8294	958	515	41326	1800	0	0	50	1997	55572	74.36
Pampas	6	191	3863	1043	1201	726	170	14411	17	7	94	679	22408	64.31
Pingao	25	57	4	0	0	6	0	0	2311	90	74	0	2567	90.03
Spinifex	312	56	0	0	0	0	0	0	165	9521	443	0	10497	90.70
Tauhinu	212	144	198	3079	0	2606	2	195	16	99	26107	1887	34545	75.57
Sedges	15	914	6073	736	992	2877	1845	1108	19	0	115	25004	39698	62.99
Column Totals	23173	11127	55070	116522	14398	53336	48305	22732	2558	10011	29207	39741	426180	
Cover Type Accuracy (%)	96.76	79.59	64.72	76.26	68.13	72.85	85.55	63.40	90.34	95.11	89.39	62.92		

March Maximum Likelihood with Vegetation Indices

Overall Accuracy = 75.77%

Kappa Coefficient = 0.7214

When the ten vegetation indices were added to the analysis, the overall accuracy only increased by 0.07% to 75.77%. The results for both March confusion indices were very similar. There was often little more than a percentage difference between the thematic class accuracy; for example, Dead Vegetation decreased in accuracy from 78.51 to 77.92, and Forest increased from 76.36 to 76.61. However, both results are within a single percentage difference and would be considered statistically insignificant.

Table 10: March Maximum Likelihood with Vegetation Indices

	Bareground	Dead Vegetation	Flax	Established Forest	Herbland	Lupin	Muelenbeckia	Pampas	Pingao	Spinifex	Tauhinu	Sedges	Row Totals	Reliability(%)
Unclassified	0	0	0	0	0	0	0	0	0	0	0	0	0	
Bareground	22515	0	0	0	0	0	0	0	2	222	64	0	22803	98.74
Dead Vegetation	252	8670	157	328	20	2160	95	205	7	64	1373	6008	19339	44.83
Flax	0	17	37224	4553	704	449	195	2392	9	0	8	2322	47873	77.76
Established Forest	0	116	2030	89273	402	4749	2726	69	0	0	101	366	99832	89.42
Herbland	2	240	6491	5378	10035	1907	1341	1847	0	0	28	1155	28424	35.30
Lupin	1	225	797	3420	32	37613	615	493	0	24	966	1474	45660	82.38
Muelenbeckia	0	320	421	9918	954	701	41295	1873	0	0	45	2089	57616	71.67
Pampas	2	138	3419	887	1438	736	216	14530	14	43	104	670	22197	65.46
Pingao	23	160	0	0	0	5	0	1	2286	86	234	0	2795	81.79
Spinifex	223	69	0	1	0	0	0	0	216	9514	271	0	10294	92.42
Tauhinu	128	81	107	2204	0	1630	2	152	1	58	25666	1370	31399	81.74
Sedges	27	1091	4424	560	813	3386	1820	1170	23	0	347	24287	37948	64.00
Column Totals	23173	11127	55070	116522	14398	53336	48305	22732	2558	10011	29207	39741	426180	
Cover Type Accuracy (%)	97.16	77.92	67.59	76.61	69.70	70.52	85.49	63.92	89.37	95.04	87.88	61.11		

Mahalanobis Distance

November Mahalanobis Distance No Vegetation Indices

Overall Accuracy = 57.44%

Kappa Coefficient = 0.5172

The following Classification algorithm was the Mahalanobis distance. These classification results were much worse than the Maximum Likelihood results analysed in the previous section. The overall accuracy of the November survey using Mahalanobis Distance was 57.44%. Pampas again had very poor accuracy (32.38%) and 24.28% of the ground truth polygons were misclassified as herbland. Herbland had an accuracy of only 26.85% and was misclassified with Muelenbeckia 21.82% and Pampas 14.89% of the time. Dead vegetation also had a very low classification accuracy of 50.30% and was consistently misclassified with Sedgeland (47.69%). Compared to the maximum likelihood classification Pingao had a great reduction in accuracy, down to 69.81, a reduction of 25.21% in accuracy. Bareground and Spinifex were the only two classes with accuracies above 80%, with 98.42% and 94.76, respectively.

Table 11: November Mahalanobis Distance No Vegetation Indices

	Sedges	Tauhini	Spinifex	Pingao	Pampas	Muelenbeckia	Lupin	Herbland	Flax	Dead Vegetation	Bareground	Established Forest	Row Totals	Reliability(%)
Unclassified	0	0	0	0	0	0	0	0	0	0	0	0	0	
Sedges	28487	1	1528	488	627	866	1201	89	2555	5	4	15829	51680	55.12
Tauhinu	9	8650	65	23	440	0	0	347	0	7	373	163	10077	85.84
Spinifex	277	1	24358	0	1282	1763	283	1850	1995	4514	0	600	36923	65.97
Pingao	16	240	401	1427	307	1	2057	284	390	160	0	20	5303	26.91
Pampas	122	0	544	0	7066	197	5102	2297	4561	5	0	107	20001	35.33
Muelenbeckia	560	0	860	0	2529	39630	391	3365	2343	2	0	48151	97831	40.51
Lupin	138	0	32	0	1970	65	52970	655	12250	0	0	4813	72893	72.67
Herbland	359	0	1566	0	5299	1013	453	4141	1856	8	0	990	15685	26.40
Flax	783	0	2226	0	1036	205	12932	788	27584	0	0	7337	52891	52.15
Dead Vegetation	0	75	8797	55	1120	221	5	1305	73	4761	0	11	16423	28.99
Bareground	495	161	0	51	2	0	3	0	2	0	23537	6	24257	97.03
Established Forest	5207	0	533	0	144	5636	2595	302	540	4	0	42392	57353	73.91
Column Totals	36453	9128	40910	2044	21822	49597	77992	15423	54149	9466	23914	120419	461317	
Cover Type Accuracy (%)	78.15	94.76	59.54	69.81	32.38	79.90	67.92	26.85	50.94	50.30	98.42	35.20		

November Mahalanobis Distance with vegetation Indices

Overall Accuracy = 58.41%

Kappa Coefficient = 0.5291

The results were similar when the Mahalanobis Distance was performed with vegetation indices. The overall accuracy increased from 57.44% to 58.41%; however, there was similar misclassification of Herbland (24.33%), Pampas (32.60%) and Dead vegetation 48.955. However, Tauhinu was classified with much higher accuracy (87.27 and an increase of 9.12%). Overall, the results remain poor, and many classes had low classification accuracies.

Table 12: November Mahalanobis Distance with vegetation Indices.

	Sedges	Tauhini	Spinifex	Pingao	Pampas	Muelenbeckia	Lupin	Herbland	Flax	Dead Vegetation	Bareground	Established Forest	Row Totals	Reliability(%)
Unclassified	0	0	0	0	0	0	0	0	0	0	0	0	0	
Sedges	31964	7	975	367	541	482	1901	49	1898	21	26	23474	61704	51.80
Tauhinu	101	8650	348	24	812	2	3	727	65	39	636	626	12034	71.88
Spinifex	256	2	25094	0	1355	2055	360	2186	2281	4582	0	637	38808	64.66
Pingao	361	268	429	1599	178	1	1363	38	345	182	0	6	4770	33.52
Pampas	217	0	490	0	7147	10	3494	1261	2607	24	0	174	15424	46.34
Muelenbeckia	297	0	1160	0	1661	39827	332	4253	1764	2	0	37786	87082	45.74
Lupin	98	0	26	0	1891	50	53868	679	12584	0	0	3393	72590	74.21
Herbland	154	2	1356	1	5816	2039	1764	3770	4732	2	0	4094	23731	15.89
Flax	834	0	2369	0	890	158	12660	682	27427	1	0	6512	51534	53.22
Dead Vegetation	1	145	8510	36	1488	231	7	1614	90	4656	0	8	16787	27.74
Bareground	98	97	0	27	0	0	0	0	0	0	21170	0	21393	98.96
Established Forest	2245	0	348	0	148	4979	2612	236	613	2	0	44277	55460	79.84
Column Totals	36627	9172	41105	2054	21926	49834	78364	15497	54408	9511	21832	120987		
Cover Type Accuracy (%)	87.27	94.31	61.05	77.84	32.60	79.92	68.74	24.33	50.41	48.95	96.97	36.60		

March Mahalanobis Distance No Vegetation Indices

Overall Accuracy = 62.11%

Kappa Coefficient = 0.5716

The accuracy percentages of the Mahalanobis Distance algorithm increased slightly in March. The overall accuracy was 62.11% compared to 57.44% for the November classification. However, Pampas still had very low accuracies (37.55%). Established Forest was also below 50 with an accuracy of 44.56; however, that improved 9.12 compared to November. Overall there was a slight improvement over the November survey; however, the accuracies were still lower than the Maximum Likelihood classification (75.70 compared to 62.11).

Table 13: March Mahalanobis Distance No Vegetation Indices.

	Sedges	Tauhini	Spinifex	Pingao	Pampas	Muelenbeckia	Lupin	Herbland	Flax	Dead Vegetation	Bareground	Established Forest	Row Totals	Reliability(%)
Unclassified	0	0	0	0	0	0	0	0	0	0	0	0	0	
Sedges	21218	362	0	44	781	1739	3293	745	4447	1516	6	334	34485	61.53
Tauhinu	2251	22694	118	22	114	113	4598	35	334	237	134	3199	33849	67.04
Spinifex	231	535	8265	117	2628	6	0	335	1	233	246	139	12735	64.90
Pingao	1307	3	24	1587	1393	74	52	403	774	49	3	8	5677	27.95
Pampas	233	330	48	8	8366	70	293	1771	721	35	5	360	12241	68.35
Muelenbeckia	1459	324	1	0	1931	40385	1365	1652	250	446	1	15712	63528	63.57
Lupin	590	1116	26	0	1875	686	35584	41	1499	78	0	17555	59050	60.26
Herbland	1643	1128	11	11	2720	1324	1864	7391	10393	171	0	13473	40130	18.42
Flax	1740	40	0	0	1892	21	448	1580	35640	31	6	16372	57770	61.69
Dead Vegetation	8220	416	81	305	557	485	1866	172	242	7846	168	240	20599	38.09
Bareground	0	1760	295	6	0	0	5	0	0	0	21562	0	23629	91.25
Established Forest	349	64	0	0	23	3083	3483	390	908	23	0	54164	62487	86.68
Column Totals	39242	28771	8870	2100	22280	47986	52852	14516	55209	10666	22132	121556		
Cover Type Accuracy (%)	54.07	78.88	93.18	75.56	37.55	84.16	67.33	50.92	64.55	73.56	97.43	44.56		

March Mahalanobis distance with Vegetation Indices

Overall Accuracy = 60.52%

Kappa Coefficient = 0.5566

Interestingly the accuracies decreased when the Mahalanobis algorithm was run for the March survey. The overall accuracy of 60.52% was recorded, a reduction of 1.59%. The Established Forest class reduced to 37.56% accuracy (a decrease of 7%). Pampas accuracy was slightly higher; however, it remained below 50% at 40.05%. Tauhinu increased to 93.35%, 14.47% higher compared to the value without vegetation indices. However, most of the classification accuracies were similar or slightly lower than those without the vegetation indices.

Table 14: March Mahalanobis distance with Vegetation Indices.

	Sedges	Tauhini	Spinifex	Pingao	Pampas	Muelenbeckia	Lupin	Herbland	Flax	Dead Vegetation	Bareground	Established Forest	Row Totals	Reliability(%)
Unclassified	0	0	0	0	0	0	0	0	0	0	0	0	0	
Sedges	19956	256	0	61	668	1864	2896	709	3961	1451	7	290	32119	62.13
Tauhinu	4148	26858	196	6	242	259	8073	78	1688	357	1058	14165	57128	47.01
Spinifex	240	767	8269	111	2241	6	18	364	42	243	257	306	12863	64.29
Pingao	1729	3	17	1596	1553	137	48	435	924	41	2	9	6494	24.58
Pampas	266	31	5	1	8924	80	191	1709	840	22	2	106	12177	73.28
Muelenbeckia	1427	79	0	0	1955	40402	624	1734	275	425	0	23292	70213	57.54
Lupin	533	188	19	0	1733	611	35407	24	1253	96	0	8268	48132	73.56
Herbland	1456	170	19	19	2495	1098	1612	7351	10121	170	1	12278	36792	19.98
Flax	1487	3	0	0	1828	20	461	1555	35032	1	11	16947	57345	61.09
Dead Vegetation	7654	335	126	298	604	460	1907	154	232	7838	169	239	20016	39.16
Bareground	0	55	219	8	0	0	0	0	0	0	20624	0	20907	98.65
Established Forest	346	26	0	0	38	3048	1615	402	842	23	0	45656	51995	87.81
Column Totals	39242	28771	8870	2100	22280	47986	52852	14516	55209	10666	22132	121556	426180	
Cover Type Accuracy (%)	50.85	93.35	93.23	76.01	40.05	84.20	66.99	50.64	63.45	73.48	93.19	37.56		

Nueral Net

Neural Net classifications had overall higher levels of accuracy than Mahalanobis distance classifications. However, the pixel-based classifications were less accurate than the Maximum Likelihood algorithm. The March classifications were again slightly more accurate than the November classifications.

November Neural Net with no Vegetation Indices

Overall Accuracy: 66.73%

Kappa Coefficient: 0.6075

The November Neural Net classification had an overall accuracy of 66.73%. In Particular, Sedges (71.48%), Spinifex (83.06%), Lupin (85.12%) and Bareground (97.76%) had a high level of accuracy. However, many classes were misclassified. The Pingao class only had an accuracy of 35.86%, while Pampas only had an accuracy of 9.61% and was consistently misclassified as Herbland (55.7% of the time). The misclassification of Pampas was significantly worse than both the Mahalanobis and Maximum Likelihood Classifications.

Table 15: November Neural Net with no Vegetation Indices.

	Sedges	Tauhini	Spinifex	Pingao	Pampas	Muelenbeckia	Lupin	Herbland	Flax	Dead Vegetation	Bareground	Established Forest	Row Totals	Reliability(%)
Unclassified	0	11	0	0	0	0	0	0	0	0	424	1532	1967	
Sedges	27596	14	566	597	273	4	907	21	348	206	12	3504	34047	81.05
Tauhinu	4	7617	0	192	0	0	0	0	0	0	25	2	7840	97.16
Spinifex	476	0	29376	4	1367	1375	771	1590	2628	5593	0	729	43909	66.90
Pingao	22	9	87	736	99	0	0	36	5	215	0	16	1227	60.03
Pampas	2	92	304	1	2108	7	387	134	308	6	0	65	3415	61.72
Muelenbeckia	146	0	642	0	1155	20737	117	2919	1278	0	0	3371	30365	68.29
Lupin	814	0	530	0	3636	173	66693	1488	24721	0	0	3912	101967	65.41
Herbland	1037	12	4407	68	12211	2006	4753	7923	7299	219	0	1969	41905	18.91
Flax	397	0	1660	0	321	4	2690	51	15951	1	0	1431	22506	70.87
Dead Vegetation	0	124	2710	404	98	3	5	6	1	3248	29	1	6629	48.99
Bareground	86	1216	0	13	0	0	3	0	0	0	21399	0	22717	94.20
Established Forest	6042	75	816	38	653	25516	2026	1325	1859	22	1	104434	142807	73.13
Column Totals	36621	9170	41099	2053	21923	49826	78352	15494	54399	9510	21890	120967		
Cover Type Accuracy (%)	75.35	83.06	71.48	35.86	9.61	41.62	85.12	51.14	29.32	34.15	97.76	86.33		

November Neural Net with Vegetation Indices

Overall Accuracy: 66.87

Kappa Coefficient: 0.6103

The results from the November flight using the Neural Net Algorithm with the Vegetation Indices included displayed similar results as the classification output without vegetation Indices. Overall accuracy increased from 66.73% to 66.87%. However, the difference is not significant, a 0.15% increase. Again, the Pampas class was consistently misclassified with an overall accuracy of only 7.04%, again Herbland (57.28%) and Lupin (18.07%) were consistently the incorrect classification output for the ground truth Pampas pixels.

As expected, the general trends of accuracy percentages for all classes were similar for both March and November classifications, including vegetation indices and the classification output. However, it could be assumed that there would be a higher level of accuracy with the additional information of the vegetation indices. These results show little influence with or without vegetation indices in the output results between the two classification runs. The tables are similar in all classification categories.

Table 16: November Neural Net with Vegetation Indices.

Class	Sedges	Tauhini	Spinifex	Pingao	Pampas	Muelenbeckia	Lupin	Herbland	Flax	Dead Vegetation	Bareground	Established Forest	Row Totals	Reliability(%)
Unclassified	0	0	0	0	0	0	0	0	0	0	69	0	69	
Sedges	28959	19	1293	724	515	35	1161	90	592	461	17	4884	38751	74.73
Tauhinu	2	7119	1	234	0	0	0	0	0	0	30	2	7388	96.36
Spinifex	264	0	27541	2	1085	1343	422	1445	1908	5408	0	493	39912	69.01
Pingao	5	4	58	632	50	0	0	7	2	68	0	5	831	76.05
Pampas	1	66	281	1	1535	6	188	87	188	8	0	53	2414	63.59
Muelenbeckia	110	0	541	0	1143	20992	78	2813	1037	0	0	3603	30317	69.24
Lupin	925	0	586	0	3944	269	66496	1569	23786	0	0	4714	102290	65.01
Herbland	977	28	4986	72	12500	2536	4547	8127	7463	287	0	2022	43546	18.66
Flax	577	0	2339	0	383	8	3537	72	17893	9	0	2406	27224	65.73
Dead Vegetation	0	68	2649	320	90	3	3	6	0	3208	28	0	6375	50.32
Bareground	97	1757	1	21	0	0	3	0	0	0	23769	0	25648	92.67
Established Forest	4536	67	634	38	577	24405	1558	1207	1280	17	1	102232	136552	74.87
Column Totals	36454	9128	40911	2044	21822	49598	77993	15423	54150	9466	23914	120414		
Cover Type Accuracy (%)	79.44	77.99	67.32	30.92	7.03	42.33	85.26	52.69	33.04	33.89	99.39	84.90		

March Neural Net without Vegetation Indices

Overall Accuracy: 72.15%

Kappa Coefficient: 0.6708

The two March classification runs of the Neural Net algorithm (with and without Vegetation Indices) had higher overall accuracy than the November runs. The first run without vegetation indices produced 72.15% compared to 66.73% in November. The Pampas Vegetation Class had a much higher accuracy than in November (32.37%); however, this value is far below an acceptable level of accuracy. The Herbland Class also had an accuracy below 50%. In addition, Pingao had an accuracy of only 13.36%.

While the Neural Net algorithm had certain classes with very high accuracies (Tauhinu (83.06%), (Spinifex 92.11%), Bareground (97.21%), Forest (84.86%)), it also had significant variability and very low accuracies for classes such as Pingao and Pampas as mentioned earlier. Therefore, caution would need to be applied when looking at the overall accuracy of this result.

Table 17: March Neural Net without Vegetation Indices.

	Sedges	Tauhini	Spinifex	Pingao	Pampas	Muelenbeckia	Lupin	Herbland	Flax	Dead Vegetation	Bareground	Established Forest	Row Totals	Reliability(%)
Unclassified	0	0	0	0	0	0	0	53	0	0	306	1363	1723	
Sedges	23401	205	0	413	2286	2976	4096	4464	4208	2285	23	526	44883	52.14
Tauhinu	2421	23801	44	2	130	0	836	0	42	243	53	1581	29153	81.64
Spinifex	146	413	8146	531	2	0	2	0	0	485	113	3	9843	82.76
Pingao	341	2	3	279	133	1	20	6	3	750	3	35	1577	17.72
Pampas	371	37	3	0	7185	33	27	217	321	6	0	79	8280	86.78
Muelenbeckia	2269	130	0	1	1891	36040	415	896	662	403	0	5841	48546	74.24
Lupin	771	1500	34	0	2274	446	31734	444	1076	341	8	2136	40764	77.85
Herbland	36	16	0	0	137	183	205	420	58	12	0	189	1256	33.42
Flax	5125	447	6	0	8006	262	3138	6560	44977	149	0	6586	75254	59.77
Dead Vegetation	3278	539	32	862	24	15	1226	16	58	5889	116	188	12243	48.10
Bareground	6	1128	576	2	1	0	0	0	3	3	21724	11	23454	92.62
Established Forest	915	436	0	0	130	7842	10930	1435	3575	61	0	103881	129205	80.40
Column Totals	39081	28655	8844	2091	22198	47797	52628	14509	54982	10627	22347	122419	426180	
Cover Type Accuracy (%)	59.88	83.06	92.11	13.36	32.37	75.40	60.30	2.89	81.80	55.41	97.21	84.86		

March Neural Net with Vegetation Indices

Overall Accuracy: 70.47%

Kappa Coefficient: 0.6568

Similar to the November study, the addition of Vegetation indices had little effect on the output classification. In March, the accuracy was reduced from 72.15% to 70.47%. Like the November study, the herbland and pingao classes had low accuracy, while tauhinu, spinifex, and Bareground had very high accuracy. Muelenbeckia had high accuracy (86.39%) however was consistently misclassified as many other vegetation classes (12.44% of Sedges Class, 18.08% Herbland Class and 15.39% of the Forest Class). The above example illustrates the importance of understanding errors of commission and omission. Therefore, it is crucial to examine confusion matrices results in a greater depth rather than focusing solely on overall accuracy percentages.

Table 18: March Neural Net with Vegetation Indices.

	Sedges	Tauhini	Spinifex	Pingao	Pampas	Muelenbeckia	Lupin	Herbland	Flax	Dead Vegetation	Bareground	Established Forest	Row Totals	Reliability(%)
Unclassified	0	0	0	0	0	0	0	53	0	0	307	1363	1723	
Sedges	18884	49	0	59	831	1835	2360	1432	2829	1630	39	325	30273	62.38
Tauhinu	779	23000	30	15	79	2	780	28	106	156	52	1316	26343	87.31
Spinifex	2	231	8018	164	0	0	0	0	0	37	76	1	8529	94.01
Pingao	83	0	18	516	3	7	3	0	5	0	1	1	638	80.94
Pampas	1165	111	4	0	14184	196	189	1742	2285	145	19	166	20207	70.19
Muelenbeckia	4862	27	0	4	2141	41287	1482	2623	3197	430	0	18842	74896	55.13
Lupin	3086	2244	31	0	1893	684	35745	1441	3825	335	1	5311	54595	65.47
Herbland	1092	560	8	19	1233	749	2058	4268	3404	224	6	1200	14822	28.80
Flax	2716	0	0	0	1707	17	838	2053	35520	46	0	3951	46848	75.82
Dead Vegetation	5890	1706	188	1237	72	10	1774	0	128	7508	141	261	18915	39.69
Bareground	1	356	537	77	0	0	0	0	0	65	21706	0	22743	95.44
Established Forest	524	371	0	0	46	3005	7409	870	3688	46	0	89689	105647	84.90
Column Totals	39083	28655	8834	2091	22190	47792	52638	14510	54986	10623	22349	122428	426180	
Cover Type Accuracy (%)	48.32	80.26	90.76	24.69	63.92	86.39	67.91	29.41	64.60	70.68	97.13	73.26		

3.3.2 Object-Based Image Analysis (OBIA) Results (eCognition Results)

November OBIA Results No Vegetation Indices

Accuracy: 77.61%

Kappa: 0.7440

The following section shows the result of the OBIA classifications. The initial results with no vegetation indices showed an overall accuracy of 77.61% (3.61% higher than the maximum likelihood and 20.17% higher than the Mahalanobis Distance. Using OBIA, Established Forest showed much higher accuracy than any pixel-based classification (90.56%). Herbland (57.74%) and pampas (54.69%) continued to have low accuracies; however, both were classified with higher accuracy than the pixel-based methods. Spinifex (88.16), Tauhinu (86.13%), Pinagao (82.78%) and Spinifex (88.15%) all continued to have higher accuracies than other classes, similar to the pixel-based analysis.

Table 19: November OBIA Results No Vegetation Indices

Classification	Dead Vegetation	Flax	Established Forest	Herbland	Lupin	Muelenbeckia	Pampas	Pingao	Bareground	Sedges	Spinifex	Tauhinu	Row Totals	Reliability(%)
Dead Vegetation	8121	75	150	187	0	187	374	0	0	3481	0	37	12613	64.39
Flax	299	56589	1272	3181	5352	1123	4154	0	0	3555	0	374	75900	74.56
Established Forest	225	1759	82899	524	973	4566	487	0	0	861	0	2021	94314	87.90
Herbland	412	2021	337	11078	1123	2283	2096	0	0	1460	0	150	20959	52.86
Lupin	112	7261	1048	2208	64336	599	2246	75	75	1048	112	1722	80841	79.58
Muelenbeckia	0	749	2844	1085	75	32598	487	0	0	1310	0	0	39148	83.27
Pampas	674	2508	599	2657	1198	1871	15270	0	0	2133	0	150	27059	56.43
Pingao	0	0	0	37	0	0	0	4678	225	0	1422	150	6512	71.84
Bareground	112	0	0	0	0	0	37	0	9806	0	636	37	10629	92.25
Sedges	2770	2171	225	1422	674	1198	2545	0	0	25038	0	150	36191	69.18
Spinifex	37	0	0	112	0	0	0	37	2320	0	17815	0	20322	87.66
Tauhinu	112	674	2171	711	936	187	225	861	75	823	225	29754	36753	80.96
Column Totals	12875	73805	91545	23204	74665	44612	27920	5651	12500	39709	20210	34544	461241	
Cover Type Accuracy (%)	63.08	76.67	90.56	47.74	86.17	73.07	54.69	82.78	78.44	63.05	88.15	86.13		

November OBIA Results No Vegetation Indices

Accuracy: 60.56%

Kappa:0.7672

Interestingly, vegetation indices' accuracy decreased dramatically compared to using only the five spectral bands. It was believed that this was an error with the bands; however, multiple re-runs and different set-up processes yield the same result. It is unclear why there is such a drop off in accuracy, as this was not observed in the March OBIA analysis. It also was not apparent in the pixel-based algorithms using the same data sets.

Table 20: November OBIA Results No Vegetation Indices

Classification	Dead Vegetation	Flax	Established Forest	Herbland	Lupin	Muelenbeckia	Pampas	Pingao	Bareground	Sedges	Spinifex	Tauhinu	Row Totals	Reliability(%)
Dead Vegetation	6838	187	224	299	262	37	1009	0	0	4185	37	1270	14348	47.66
Flax	224	35647	4858	5007	11434	1943	4932	0	0	3587	0	1644	69276	51.46
Established Forest	149	5904	64643	1607	2989	6987	747	0	0	1681	0	4334	89042	72.60
Herbland	673	3139	1532	7361	1383	2205	3064	0	0	1569	0	224	21149	34.81
Lupin	598	13003	3213	3101	58739	336	4185	75	112	3326	37	1420	88145	66.64
Muelenbeckia	224	2989	7959	2728	262	21261	598	0	0	1084	0	673	37777	56.28
Pampas	1046	3774	1270	4297	2728	1719	10126	0	0	2690	37	673	28361	35.70
Pingao	75	0	0	0	0	0	0	3587	224	0	2205	262	6352	56.47
Bareground	411	0	0	0	0	0	0	37	9566	0	560	37	10612	90.14
Sedges	3961	2317	2242	4035	2616	374	3027	0	0	18197	0	2205	38972	46.69
Spinifex	374	0	0	37	0	0	37	299	1532	0	17039	0	19318	88.20
Tauhinu	336	1495	5082	635	673	374	187	859	37	1719	187	26305	37889	69.43
Column Totals	14909	68454	91023	29108	81083	35236	27912	4858	11471	38038	20103	39047	461241	
Cover Type Accuracy (%)	45.86	52.07	71.02	25.29	72.44	60.34	36.28	73.85	83.39	47.84	84.76	67.37		

March OBIA Results No Vegetation Indices

Accuracy : 80.09%

Kappa : 0.7672

The March OBIA result showed the highest overall accuracy seen yet of 80.09%. In particular, pampas scored 77.76% correctly compared to the pixel-based analyses and consistently yielded results below 50%. The only two thematic classes with low accuracy percentages were sedges (33.79%) and herbland (53.72%). Sedgeland was consistently misclassified with flax (22.59%), while herbland was also misclassified with flax (15.35%) and forest (10.15%).

Table 21: March OBIA Results No Vegetation Indices

Classification	Dead Vegetation	Flax	Establishe Forest	Herblan	Lupin	Muelenbeckia	Pampas	Pingao	Bareground	Sedges	Spinifex	Tauhinu	Row Totals	Reliability(%)
Dead Vegetation	7174	29	206	265	1117	764	470	29	382	1705	88	382	12613	56.88
Flax	147	61328	1323	3822	2234	353	2969	59	0	3381	0	88	75705	81.01
Establish Forest	147	2587	95491	2528	3263	3675	206	0	29	853	0	764	109544	87.17
Herbland	88	2029	706	13377	382	323	882	0	0	294	0	0	18081	73.98
Lupin	676	382	4469	1147	52538	1205	206	0	29	1617	0	1793	64062	82.01
Muelenbeckia	29	206	4351	1382	794	36426	88	0	0	1117	0	0	44394	82.05
Pampas	88	3528	588	1558	1382	1911	18199	0	29	500	0	265	28047	64.88
Pingao	647	0	0	0	0	29	29	5851	29	29	1235	176	8026	72.89
Bareground	265	0	0	59	29	29	29	0	5645	88	147	265	6556	86.10
Sedges	911	764	323	676	1705	1352	265	0	0	5057	0	147	11201	45.14
Spinifex	118	0	0	0	59	0	0	59	1058	0	15435	118	16846	91.62
Tauhinu	441	118	1235	88	2764	59	59	29	970	323	206	24813	31105	79.77
Column Totals	10731	70971	108691	24902	66267	46128	23402	6027	8173	14965	17111	28812	426180	
Cover Type Accuracy (%)	66.85	86.41	87.86	53.72	79.28	78.97	77.76	97.07	69.06	33.79	90.21	86.12		

March OBIA Results with Vegetation Indices

Accuracy : 79.90%

Kappa : 0.7674

The March OBIA results with vegetation indices were almost identical to the results without vegetation indices (79.90% overall accuracy). Again, this is in stark difference from the anomaly of the results recorded with the November study. Herbland showed similar accuracies 51.88%, a decrease of 1.84% from the November study). One interesting thing to note was that Sedges dramatically increased accuracy compared to the November classification up to 68.69% from 33.79% in November). It was still confused with Flax 10.44% of the time, but this is a significant increase in accuracy compared to the November study.

Table 22: March OBIA Results with Vegetation Indices

Classification	Dead Vegetation	Flax	Establishe Forest	Herblan	Lupin	Muelenbeckia	Pampas	Pingao	Bareground	Sedges	Spinifex	Tauhinu	Row Totals	Reliability(%)
Dead Vegetation	6892	28	195	195	1116	726	446	28	391	1646	84	223	11971	57.58
Flax	167	58292	1172	3795	2037	335	2651	56	0	3209	0	140	71853	81.13
Established Forest	140	2456	90605	2372	3153	3460	223	0	28	781	0	753	103971	87.14
Herbland	84	1897	670	12724	307	335	837	0	0	307	0	0	17161	74.15
Lupin	614	391	4381	1116	49530	1228	195	0	28	1591	0	1730	60803	81.46
Muelenbeckia	56	167	3739	1395	726	34852	84	0	0	1116	0	0	42135	82.72
Pampas	112	3404	586	1423	1200	1758	17356	0	28	502	0	251	26621	65.20
Pingao	502	0	0	0	0	28	28	5665	56	28	1172	187	7665	73.90
Bareground	223	0	0	84	28	28	0	0	5385	112	112	251	6223	86.55
Sedges	1646	1618	502	1311	3125	1814	558	0	56	21123	0	558	32313	65.37
Spinifex	84	0	0	0	56	0	0	28	1032	0	14650	140	15989	91.62
Tauhinu	419	140	949	112	2902	28	56	56	865	335	223	23439	29523	79.40
Column Totals	10938	68393	102799	24528	64180	44591	22435	5832	7869	30750	16240	27673	426228	
Cover Type Accuracy (%)	63.01	85.23	88.14	51.88	77.17	78.16	77.36	97.13	68.44	68.69	90.21	84.70		

3.4 Output Classification Maps

All of the classification algorithms produced classification maps of Karekare. Figures 30 and 31 illustrate a sample of these results. The classification maps are the result of the maximum likelihood classification, and it shows a visual indication of how the vegetation coverage has changed between November and March. For example, in Figure 31, it can be seen the extent of spinifex in the foredunes has dramatically increased. In addition, there is also more Lupin in the places where Muelenbeckia occupied this space in the November classification.

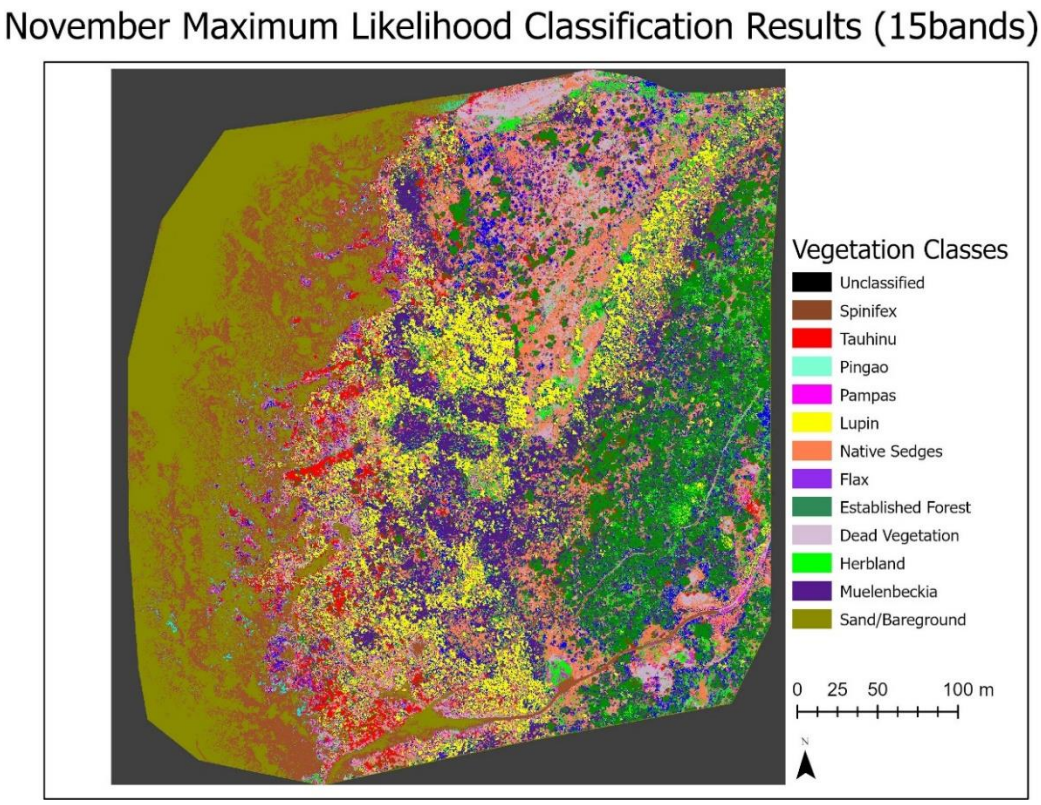

Figure 30:November Maximum Likelihood Classification Results in map format

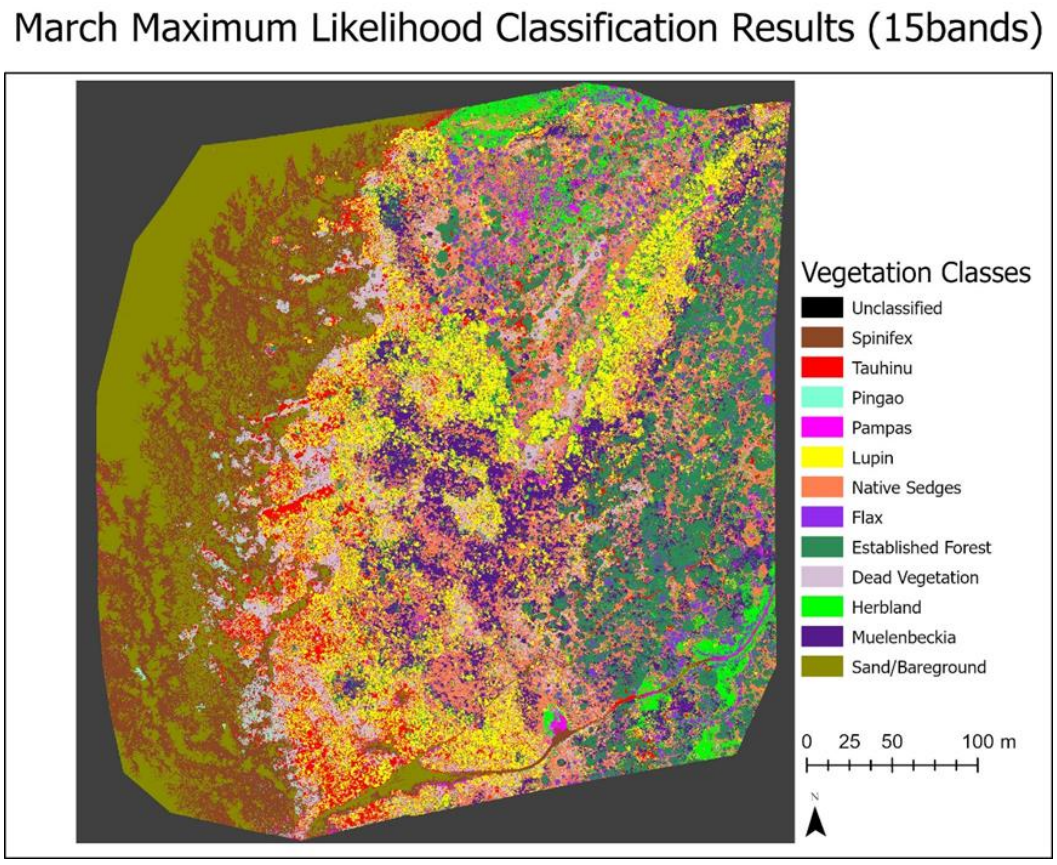

Figure 31: March Maximum Likelihood Classification Results in map format

4. Discussion

4.1 Pixel-Based and OBIA algorithm comparison

A principal goal in this research was to compare and contrast pixel-based and OBIA classification models advantages and disadvantages using UAV methods. The results showed a slight increase in overall accuracy using OBIA methods compared to pixel-based methods. For example, results without Vegetation indices showed accuracies of 77.61% and 80.09% for the November and December OBIA classifications, respectively. Compared to the most accurate pixel-based methods (Maximum Likelihood) of 74.00% and 75.70%, an increase of 3.61% and 4.39% was observed using the same five-band input (without vegetation indices). Possible reasons for this increase included shape, texture, spatial relationship and other underlying differences in OBIA methodology.

This increase in overall accuracy from OBIA classification methods provides a promising indication of the potential OBIA classification methods can have in future Remote Sensing projects. However, it is essential to note that this study's overall increase in accuracy is relatively small and inconsistent for all the thematic classes observed. For example, pampas had a producer accuracy of 52.87% and a user accuracy of 54.69%. In contrast, other thematic classes had much higher values, such as established forest (87.60% and 90.56%) for producer and user accuracies, respectively. Additional examples of differences in thematic classes can be observed in the results section. Possible reasons for the low accuracy in pampas can be linked back to the similar spectral signatures of pampas with muelenbeckia, herbland and flax. This remains a consistent challenge in remote sensing: the balance between differentiating thematic classes concerning the purpose and objective of the study and the real-world spectral, textural and spatial relationship difference that classification algorithms can account for (Cruzan et al., 2016).

Pampas is a highly invasive species prominent within many New Zealand coastal ecosystems (Holliston & Dagmar, 2017). However, identifying this is very difficult due to the spectral similarities with other species. Pampas consistently had a low producer and user accuracy in all of the classification schemes compared to other thematic classes. It was hoped that the distinctive shape and texture of pampas could be used in OBIA classification methods to increase the accuracy of this thematic class. The digitisation of the overall shape of the pampas plant and the inclusion of additional textural and spatial attributes would increase the overall accuracy of this thematic class. However, it provided a challenge in all methods of automatic classification.

However, while some thematic classes provided consistently low accuracies regardless of the classification algorithm, the overall increase in accuracy from OBIA classifications compared to pixel-based classification is encouraging. Of equal importance is the ability of the Maximum Likelihood classification to provide consistently high overall levels of accuracy for all four study flights. OBIA classification is a very time-consuming process and requires a lot of pre-existing knowledge to carry out (Blaschke, 2010). The ability of a pixel-based classification algorithm to provide such consistent results without the additional information afforded by OBIA classification was impressive.

OBIA classification requires a lot of user input and variables such as scale parameter, shape/colour weighting and object compactness (Mafanya et al., 2017). These variables are user allocated within the eCognition software and can lead to differences in studies between two researchers who have been supplied the same data. In this study, the Estimation of Scale Parameter (ESP) was used to determine the best scale for the project (Dragut et al., 2010). However, even with this additional information, the user must decide appropriate values for each of the three user-controlled variables. The variability was minimised by providing a step-guide of best practices in the methods section.

OBIA is an emerging technology, and there have been numerous recent studies implementing OBIA classification algorithms into their studies (Blaschke., 2013). The additional information OBIA provides compared to solely spectral pixel-based algorithms is reason to be optimistic about the continued development of this technology for a wide variety of studies.

4.2 Temporal Variability

The seasons' effects of the two studies were stark. The March results had higher accuracy than the November results in every classification technique using the same algorithm. Possible reasons for this difference include the flowering of many species within the study site lupin, manuka and kanuka. Other studies have corroborated this theory that vegetation in flower can be more effectively classified. The findings seem logical as it is much easier for the naked eye to differentiate tree lupin with its distinctive yellow flowers than other low shrub and tree species.

Another reason for the difference in classification accuracies was the weather in the weeks before the March flights. The previous months were very dry, and, therefore, a significant proportion of the vegetation no longer had very high NDVI values. In November, many of the vegetation species had high values of NDVI, making it very difficult to differentiate spectrally between them. However, in March, the differences in NDVI between species was exaggerated, and therefore the classification algorithms were more effective in allocating thematic classes.

For temporal/ seasonal studies to be undertaken, a radiometric correction was needed to be carried out (Ibqual et al., 2018). This study aimed to provide a numerical guideline of spectral and object-based values relatively autonomously to future studies. However, the output spectral values between the November and March spectral signatures within the same

thematic class varied dramatically in practice. Therefore, a standardised guideline of values and rulesets within an Object-based thematic classification was not applicable. Possible reasons for the discrepancies include weather-based vegetation health and condition and natural variability of spectral signatures seasonally.

However, an additional reason for the changes was the radiometric calibration itself. All radiometric panel values were specific to the panel serial number identified and calibrated by the manufacturer. However, in practice, when inputting this value into the photogrammetry software (Pix4D) overall image had a lower value in reflectance that seemed not solely attributed to seasonal differences in the vegetation as some of the consistent values (sand and bare ground) showed differences also. The UAV had a sunlight indicator that was fully operational during all of the flights, and many tests were carried out to ensure the validity of the results. All the radiometric calibration inputs were functional and followed proven methodologies of radiometric calibration. However, exact radiometric calibration for a small UAV is complicated given the large number of variables that can affect the outcome.

Overall, it can be determined that the use of exact spectral numbers for automated vegetation classification is not applicable with current technology using the methodology outlined in this study. In addition to limitations of algorithms to account for all possible influences, many local variables explain that exact predetermined/ numerical automation is not applicable. While some variation was expected prior to this study, it was hoped that radiometric calibration could account for these differences. However, future multi-annual studies during similar dates in the year would provide additional information on the viability of radiometric calibration using the same methodology outlined in this study.

4.3 The overall effectiveness of UAVs for Vegetation Monitoring and Classification

While numerical guidelines for rulesets seem to be not applicable within UAV-based studies of vegetation classification, there are additional positive learnings from this study. The ruleset and methodology used for eCognition are repeatable and produced a relatively high overall accuracy (77.61% and 80.09% for November and March OBIA results without vegetation indices included). The current methodology in this study involves using ground truth, field-collected data that is subsequently digitised. This is a proven and widely implemented method of remote-sensing classification. Indeed, the time taken for a sample subset of training/ground data to be collected is much less than the time needed for a total field-based vegetation sample. The overall accuracies of the study suggest that there is a great deal of promise in methodologies similar to the one implemented in this research.

In general, the accuracy of remote sensing classification is inversely correlated to the number of thematic classes included in a study (Schowengerdt., 2006). The larger the number of thematic classes, the higher the probability of misclassification. In this study, certain thematic classes were consistently misclassified; an example of this was herbland which consistently had accuracy percentages around 50% for all the classification algorithms implemented, both pixel-based and object-based. This class combines grass species with wide variability in NDVI depending on plant health. Misclassification of the herbland class was not solely related to a single thematic class and was misclassified as lupin, muelenbeckia, flax and sedges amongst other thematic classes.

Other vegetation classes, such as pampas, showed low values of accuracy. Therefore, the ability of UAV-based remote sensing vegetation classification is determined by the acceptable level of accuracy required for a given project (Jensen., 2000). For identifying single pest/invasive species, such as pampas, a more targeted approach involving presence/absence classification would be more appropriate. In this study, a balanced

approach to thematic class allocation was undertaken, involving the separation of thematic classes via spectral variability – diagnosed in the preliminary investigation. Key species representing ecological health were of equal importance, such as invasive pest species (lupin and pampas) and native species of high ecological significance (muelenbeckia, pingao and spinifex).

The overall accuracies of the study would be increased if this study only included thematic classes based upon differences in spectral signatures or a reduction in thematic classes. However, information regarding the ecological health and condition of the study site would be reduced. A subtle balance of the two diverging inputs needs to be considered. However, overall accuracies and high percentage accuracies of certain thematic classes such as pingao, spinifex and tauhinu are promising for future studies. While there are many ways thematic classifications can be allocated, the importance of understanding the project's overall goals should always be accounted for.

4.4 Advantages and Disadvantages of Current Technology with a look to the future

4.4.1 UAV Technology

This study used the phantom 4-Pro UAV with the MicaSense Red-Edge sensor attached. This sensor is widely used in various disciplines for vegetation analysis, including agriculture, forestry and environmental research (Taddia et al., 2020; Olsen & Anderson, 2021 etc.). The ability of this sensor to capture near infra-red and red-edge spectral signatures provides a lot of additional information to the user and for the classification algorithms. However, while multispectral analysis provides additional spectral information, generally, there is a sacrifice in resolution and visual fidelity compared to traditional RGB camera lenses. Indeed, the Red-Edge sensor has an overall resolution of 1.2 megapixels compared to the camera onboard the Phantom 4-pro, which has a resolution of 20 megapixels.

The relatively low resolution of the Red-Edge sensor resulted in some difficulties identifying the outlines of the vegetation when related to the corresponding field analysis. However, with continued advancement in camera lens technology, the increase in resolution and spectral information in multispectral sensors will increase the viability of UAV-based vegetation analysis.

The Phantom 4-pro has a flight time of between 25 and 30 minutes without the sequoia sensor attached. However, the increased weight of this sensor reduced each flight to around 15-18 minutes. Further advancements to UAV technology and a reduction of weight on the sensor will increase the spatial extent of future studies. However, for studies involving a relatively small area, current technologies for UAV research still provide decent aerial coverage.

In addition to the flight time and resolution of the UAV, advancements in the technology used for radiometric calibration has been identified as a key factor in the ability to provide accurate results to the end-user. Improvements to the sunlight sensor on the drone and algorithms for radiometric calibration will reduce any potential inaccuracies caused by changing atmospheric conditions. Atmospheric conditions can change rapidly and vary greatly seasonally; therefore, advancements in this technology are equally important for improving UAV-based studies' accuracy as the previously mentioned resolution increases.

4.4.2 Software and Classification Algorithms

This study used a variety of classification algorithms. Many studies, especially very high-resolution Studies such as UAV-based research, have implemented OBIA algorithms instead of pixel-based (De Castro et al., 2018). As mentioned previously, this study showed an overall increase in accuracy using OBIA-based methodology. However, OBIA is very complex, and several variabilities need to be accounted for. eCognition software is used in

many research projects; however, additional software such as Feature Analyst for ArcGIS is available (Lourenço et al., 2021). Other studies use purpose-built OBIA classification algorithms and techniques created by researchers (Cui et al., 2021).

OBIA is an emerging field in scientific literature, and future advancements in algorithms and techniques should increase the accuracy of this field (Hossain & Chen., 2019). While eCognition has a learning curve, the workflow provided in the methods section offers an overview for end-user to apply this to their chosen research topic. The increasing prevalence of OBIA in research should lead to further advancements. Not only for increasing the accuracy of the output research but provide a researcher new to the field with a wide variety of sources to identify the best methodologies used for their study. It is hoped that the workflow created in the methods section will provide a basis for future research that can be adapted for future research. While ease of use is much greater for pixel-based analysis, the overall trend in environmental research is an increased number of studies in OBIA analysis. This field's increased prevalence and adoption are the key advantages and additional information related to shape, outline, and spatial relationships. Therefore, it would be expected that this field should continue to grow, and methods of best practices and methodologies for a wide variety of OBIA studies will be created

4.4.3 Optical Sensors vs LiDAR

This study used UAV-based optical sensors for the analysis. Optical sensors work well to create a 2-D orthomosiac; however, they do not function well when creating a 3-D model. Similar challenges in creating a 3-D model of sand dunes using optical sensors were faced in Moloney et al.'s (2018) study. Attempts were made to create a 3-D model using photogrammetry; however, errors in elevation and holes where the model failed to have

enough points for the point cloud mesh meant that this section of the analysis was abandoned in this study.

For more accurate 3-D models of an environment, LiDAR technology is much more suitable (Sofonia et al., 2019). LiDAR has the advantage of reading both first and second responses from the sensor, which allows vegetation removal from a model to create an accurate Digital Elevation Model (DEM) (Shaw et al., 2019). In addition to removing vegetation, LiDAR technology is much more accurate for elevation models and is the industry standard for creating 3-D DEMs. Recent technological advantages in LiDAR sensor technology have reduced the size and weight of the sensor, and therefore, LiDAR mounted UAVs can dramatically change many research studies.

5. Conclusion

There were five goals this thesis aimed to achieve:

To compare the use of pixel-based and object-based classifications for analysing high-resolution data. Second, to provide a case study of how seasonal and temporal effects influence vegetation classification accuracy. Third, assess UAVs viability for vegetation surveys and classification maps. Fourth, create a detailed workflow and list of best practices for using UAVs to create a vegetation classification map. Finally, evaluate the advantages and limitations of current technology for vegetation surveys.

5.1 Pixel and Object-based Findings

The object-based classification gave slightly higher accuracies than pixel-based. However, the Maximum Likelihood classification with no vegetation indices had accuracies of 75.70% and 74.00% for the November and March surveys, respectively. These accuracies were less than 77.61% and 80.09% for the OBIA classifications without vegetation indices. The increase in accuracy of the OBIA could be attributed to the additional data provided to the classification algorithms. The increase in accuracy of the OBIA study is promising, and there has been a trend of increased studies using OBIA methods compared to pixel-based studies (Ye., 2018). The other two pixel-based methods (Neural Net and Mahalanobis Distance) consistently produced lower accuracy than the Maximum Likelihood and OBIA methods.

5.2 Seasonal/ Temporal Findings

The accuracies produced in the March Survey were higher than the November Survey for all classification algorithms. The spectral profiles of the March flight showed more significant variability, increasing the ability of the classification algorithms to differentiate thematic classes. The March Survey occurred after many weeks with low volumes of water, and therefore the difference in NDVI specifically was exaggerated compared to the November survey. The result shows the great temporal and seasonal effects that influence the accuracy

of a vegetation survey. In addition, when certain species are flowering, such as (lupin and spinifex in March), it becomes easier to identify these species. There may be vastly different spectral signatures depending on the time of year or health of the plant.

In this study, high overall accuracies were achieved using OBIA methods. In March, pampas especially had much higher accuracy when using OBIA methods than traditional pixel-based methods. The additional information of shape and textural properties provided in OBIA classification has been shown to be a significant factor in increasing the accuracies of some thematic classes. However, pampas was below 50% in both November classifications. The variance exemplifies the different seasonal factors can have on a vegetation survey and the complexities of the classification algorithms. While OBIA is more adept at identifying pampas, it failed to produce acceptable accuracy in November. This study's seasonal and temporal differences were stark, and the influence of timing vegetation surveys needs to be carefully considered.

5.3 UAVs Viability for Vegetation Classification

UAVs reduce the time and potential environmental impact of field surveys. They also provide high-resolution data at a fraction of the cost of aerial photography and with resolutions much higher than satellite imagery. However, they do lose the detail of identifying tens or hundreds of plant species that field sampling can provide. However, it can be a highly effective tool to identify key target species. In this study 12 thematic classes were used; however, other studies targeting specific pests or native species could be highly effective. Within the 12-class structure, the results showed certain thematic classes with low overall accuracies. Reducing the thematic classes could be a more effective solution, especially for pest management. However, the overall accuracy created from OBIA classification was high and showed the

promise of complete vegetation surveys using only UAV. However, ideally, these would be supplemented by a detailed field survey of a section of the coastal dune.

5.4 A Detailed workflow and list of best practices

A workflow and a list of best practices are provided in the methods section. The workflow for UAV flight and safety precautions can be applied to any remote sensing study. In addition, the methodology used in eCognition can be used as a starting point for future studies. This study provides only a small glimpse of the workflows and rulesets that can be created in eCognition or other OBIA based algorithms.

5.5 Advantages and Limitations of current technologies

The technology of sensors and UAVs are constantly evolving. There have been recent studies with LiDAR mounted UAVs (Donager et al., 2021) and hyperspectral sensors (Centeno et al., 2020). As technology advances, remote sensing applications widen and open more possibilities. For example, multispectral sensors with increased Megapixel values should create the opportunity for high resolution and high accuracy UAV-based vegetation maps. This thesis provides a brief outline and observation of UAV-based vegetation surveys. With increased scientific studies and advancements in technology, the viability of UAVs for vegetation mapping is only going to increase.

6. Reference List

Awange, J. L., & Kyalo Kiema, J. B. (2013). Fundamentals of remote sensing. In *Environmental Geoinformatics* (pp. 111-118). Springer.

Baatz, M., Schäpe, A., Strobl, J., Blaschke, T., & Griesebner, G. (2000). Multiresolution Segmentation-an optimization approach for high quality multi-scale image segmentation. Angewandte Geographische Informationsverarbeitung, 12, 12–23. Retrieved from internal-pdf.*xn--baatz_schpe_2000-3891068462-jkc/Baatz_Sch*.

Baghdadi, N., & Zribi, M. (2016). *Land surface remote sensing in continental hydrology*. Elsevier.

Barrows, C. W., Allen, E. B., Brooks, M. L., & Allen, M. F. (2009). Effects of an invasive plant on a desert sand dune landscape. *Biological Invasions*, *11*(3), 673-686.

Blaschke, T. (2010). Object based image analysis for remote sensing. *ISPRS Journal of Photogrammetry and Remote Sensing*, *65*(1), 2-16.

Blaschke, T. (2013). Object based image analysis: A new paradigm in remote sensing. ASPRS Annual Conference, March.

Blue, B., & Kench, P. S. (2017). Multi-decadal shoreline change and beach connectivity in a high-energy sand system. *New Zealand journal of marine and freshwater research*, *51*(3), 406-426.

Bolyn, C., Michez, A., Gaucher, P., Lejeune, P., & Bonnet, S. (2018). Forest mapping and species composition using supervised per pixel classification of Sentinel-2 imagery. *Biotechnologie, Agronomie, Société et Environnement*, *22*(3), 16.

Brown, A. C., & McLachlan, A. (2002). Sandy shore ecosystems and the threats facing them: some predictions for the year 2025. *Environmental Conservation*, *29*(1), 62-77.

Centeno, J., Kerm, J., Mitishita, E., & Palma, M. (2020). Pca Band Selection Method For A Hyperspectral Sensors Onboard An Uav. 2020 IEEE Latin American GRSS & ISPRS Remote Sensing Conference (LAGIRS),

Chutia, D., Bhattacharyya, D., Sarma, K. K., Kalita, R., & Sudhakar, S. (2016). Hyperspectral remote sensing classifications: a perspective survey. *Transactions in GIS*, *20*(4), 463-490.

Cockayne, L. (1911). *Report on the dune-areas of New Zealand: Their geology, botany, and reclamation*. J. Mackay, Government printer.

Cruzan, M. B., Weinstein, B. G., Grasty, M. R., Kohrn, B. F., Hendrickson, E. C., Arredondo, T. M., & Thompson, P. G. (2016). Small unmanned aerial vehicles (micro-UAVs, drones) in plant ecology. *Applications in Plant Sciences*, *4*(9), 1600041.

Cui, W., Yao, M., Hao, Y., Wang, Z., He, X., Wu, W., Li, J., Zhao, H., Xia, C., & Wang, J. (2021). Knowledge and Geo-Object Based Graph Convolutional Network for Remote Sensing Semantic Segmentation. *Sensors*, *21*(11), 3848.

De Castro, A. I., Jiménez-Brenes, F. M., Torres-Sánchez, J., Peña, J. M., Borra-Serrano, I., & López-Granados, F. (2018). 3-D characterization of vineyards using a novel UAV imagery-based OBIA procedure for precision viticulture applications. *Remote Sensing*, *10*(4), 584.

De Giglio, M., Goffo, F., Greggio, N., Merloni, N., Dubbini, M., & Barbarella, M. (2017). Satellite and unmanned aerial vehicle data for the classification of sand dune vegetation. *International Archives of the Photogrammetry, Remote Sensing & Spatial Information Sciences*, *42*.

Defeo, O., McLachlan, A., Schoeman, D. S., Schlacher, T. A., Dugan, J., Jones, A., Lastra, M., & Scapini, F. (2009). Threats to sandy beach ecosystems: a review. *Estuarine, coastal and shelf science*, *81*(1), 1-12.

Donager, J., Sankey, T. T., Meador, A. J. S., Sankey, J. B., & Springer, A. (2021). Integrating airborne and mobile lidar data with UAV photogrammetry for rapid assessment of changing forest snow depth and cover. *Science of Remote Sensing*, *4*, 100029.

Drăguţ, L., Tiede, D., & Levick, S. R. (2010). ESP: a tool to estimate scale parameter for multiresolution image segmentation of remotely sensed data. *International Journal of Geographical Information Science*, *24*(6), 859-871.

eCognition Developer, T. (2014). 9.0 User Guide. *Trimble Germany GmbH: Munich, Germany*.

French, K., Mason, T. J., & Sullivan, N. (2011). Recruitment limitation of native species in invaded coastal dune communities. *Plant Ecology*, *212*(4), 601-609.

Golubiewski, N. E., & Wessman, C. A. (2010). Discriminating urban vegetation from a metropolitan matrix through partial unmixing with hyperspectral AVIRIS data. *Canadian Journal of Remote Sensing*, *36*(3), 261-275.

Gruszczyński, W., Matwij, W., & Ćwiąkała, P. (2017). Comparison of low-altitude UAV photogrammetry with terrestrial laser scanning as data-source methods for terrain covered in low vegetation. *ISPRS Journal of Photogrammetry and Remote Sensing*, *126*, 168-179.

Haddad, N. M., Brudvig, L. A., Clobert, J., Davies, K. F., Gonzalez, A., Holt, R. D., Lovejoy, T. E., Sexton, J. O., Austin, M. P., Collins, C. D., Cook, W. M., Damschen, E. I., Ewers, R. M., Foster, B. L., Jenkins, C. N., King, A. J., Laurance, W. F., Levey, D. J., Margules, C. R., . . . Townshend, J. R. (2015). Habitat fragmentation and its lasting impact on Earth Ecosystems. *Science Advances*, *1*(2), https://doi.org/doi:10.1126/sciadv.1500052

Hamill, P., & Ballance, P. (1985). Heavy mineral rich beach sands of the Waitakere coast, Auckland, New Zealand. *New Zealand journal of geology and geophysics*, *28*(3), 503-511.

Hayward, B.W. (2017). Out of the ocean, into the fire: history in the rocks, fossils and landforms of Auckland, Northland and Coromandel. Wellington, New Zealand: *Geoscience Society of New Zealand.*

Hesp, P. (2000). Coastal sand dunes: form and function. *Forest Research, CDVN technical bulletin; 4*

Hilton, M., Duncan, M., & Jul, A. (2005). Processes of Ammophila arenaria (marram grass) invasion and indigenous species displacement, Stewart Island, New Zealand. Journal of *Coastal Research*, 21(1), 175-185.

Hilton, M., & Harvey, N. (2002). Management Implications of Exotic Dune Grasses on the Sir Richard Peninsula South Australia.

Hilton, M., Macauley, U., & Henderson, R. (2000). *Inventory of New Zealand's active dunelands*. Department of Conservation Wellington.

Hilton, M. J. (2006). The loss of New Zealand's active dunes and the spread of marram grass (Ammophila arenaria). *New Zealand Geographer*, *62*(2), 105-120.

Hossain, M. D., & Chen, D. (2019). Segmentation for Object-Based Image Analysis (OBIA): A review of algorithms and challenges from remote sensing perspective. *ISPRS Journal of Photogrammetry and Remote Sensing*, *150*, 115-134.

Houliston, G. J., & Goeke, D. F. (2017). Cortaderia spp. in New Zealand: patterns of genetic variation in two widespread invasive species. *New Zealand Journal of Ecology*, *41*(1), 107-112.

Hugenholtz, C. H., Levin, N., Barchyn, T. E., & Baddock, M. C. (2012). Remote sensing and spatial analysis of aeolian sand dunes: A review and outlook. *Earth-science reviews*, *111*(3-4), 319-334.

Iqbal, F., Lucieer, A., & Barry, K. (2018). Simplified radiometric calibration for UAS-mounted multispectral sensor. *European Journal of Remote Sensing*, *51*(1), 301-313.

Kaliraj, S., Chandrasekar, N., & Ramachandran, K. (2017). Mapping of coastal landforms and volumetric change analysis in the south west coast of Kanyakumari, South India using remote sensing and GIS techniques. *The Egyptian Journal of Remote Sensing and Space Science*, *20*(2), 265-282.

Kaneko, K., & Nohara, S. (2014). Review of effective vegetation mapping using the UAV (Unmanned Aerial Vehicle) method. *Journal of Geographic Information System*, *6*(06), 733.

Kim, M., Madden, M., & Warner, T. A. (2009). Forest type mapping using object-specific texture measures from multispectral Ikonos imagery. *Photogrammetric Engineering & Remote Sensing*, *75*(7), 819-829.

King, D. N., Nichol, S. L., & Hume, T. M. (2006). Rapid onshore sand flux in a high energy littoral cell: Piha Beach, New Zealand. *Journal of coastal research*, *22*(6), 1360-1369.

Li, M., Zang, S., Zhang, B., Li, S., & Wu, C. (2014). A review of remote sensing image classification techniques: The role of spatio-contextual information. *European Journal of Remote Sensing*, *47*(1), 389-411.

Lourenço, P., Teodoro, A. C., Gonçalves, J. A., Honrado, J. P., Cunha, M., & Sillero, N. (2021). Assessing the performance of different OBIA software approaches for mapping invasive alien plants along roads with remote sensing data. *International Journal of Applied Earth Observation and Geoinformation*, *95*, 102263.

Ma, L., Li, M., Ma, X., Cheng, L., Du, P., & Liu, Y. (2017). A review of supervised object-based land-cover image classification. *ISPRS Journal of Photogrammetry and Remote Sensing*, *130*, 277-293.

Mafanya, M., Tsele, P., Botai, J., Manyama, P., Swart, B., & Monate, T. (2017). Evaluating pixel and object based image classification techniques for mapping plant invasions from UAV derived aerial imagery: Harrisia pomanensis as a case study. *ISPRS Journal of Photogrammetry and Remote Sensing*, *129*, 1-11.

Mateen, M., Wen, J., & Nasrullah, M. A. A. (2018). The Role of Hyperspectral Imaging: A Literature. *International Journal of Advanced Computer Science and Applications*, *9*(8), 12.

Maxwell, A. E., Warner, T. A., & Fang, F. (2018). Implementation of machine-learning classification in remote sensing: An applied review. *International Journal of Remote Sensing*, *39*(9), 2784-2817.

Moloney, J. G., Hilton, M. J., Sirguey, P., & Simons-Smith, T. (2018). Coastal dune surveying using a low-cost remotely piloted aerial system (RPAS). *Journal of coastal research*, *34*(5), 1244-1255.

Müllerová, J., Pergl, J., & Pyšek, P. (2013). Remote sensing as a tool for monitoring plant invasions: Testing the effects of data resolution and image classification approach on the detection of a model plant species Heracleum mantegazzianum (giant hogweed). *International Journal of Applied Earth Observation and Geoinformation*, *25*, 55-65.

Olson, D., & Anderson, J. (2021). Review on unmanned aerial vehicles, remote sensors, imagery processing, and their applications in agriculture. *Agronomy Journal*, *113*(2), 971-992.

Partridge, T. (1992). Vegetation recovery following sand mining on coastal dunes at Kaitorete Spit, Canterbury, New Zealand. *Biological Conservation*, *61*(1), 59-71.

Perrings, C. A. (2012). Biodiversity Conservation: Problems and Policies. *Papers from the Biodiversity Programme Beijer International Institute of Ecological Economics Royal Swedish Academy of Sciences* (Vol. 4). Springer Science & Business Media.

Pix4D (2018) Pix4D User manual, *retrieved from https://support.pix4d.com/hc/en-us/sections/360003718992-Manual on 01/12/221*.

Pourazar, H., Samadzadegan, F., & Dadrass Javan, F. (2019). Aerial multispectral imagery for plant disease detection: Radiometric calibration necessity assessment. *European Journal of Remote Sensing*, 52(sup3), 17-31.

Richards, J. A., & Richards, J. (1999). *Remote sensing digital image analysis* (Vol. 3). Springer.

Richter, N., Staenz, K., & Kaufmann, H. (2008). Spectral unmixing of airborne hyperspectral data for baseline mapping of mine tailings areas. *International Journal of Remote Sensing*, *29*(13), 3937-3956.

Rossi, G., Tanteri, L., Tofani, V., Vannocci, P., Moretti, S., & Casagli, N. (2018). Multitemporal UAV surveys for landslide mapping and characterization. *Landslides*, *15*(5), 1045-1052.

Ruessink, B., Arens, S., Kuipers, M., & Donker, J. (2018). Coastal dune dynamics in response to excavated foredune notches. *Aeolian Research*, *31*, 3-17.

Scarelli, F. M., Sistilli, F., Fabbri, S., Cantelli, L., Barboza, E. G., & Gabbianelli, G. (2017). Seasonal dune and beach monitoring using photogrammetry from UAV surveys to apply in the ICZM on the Ravenna coast (Emilia-Romagna, Italy). *Remote Sensing Applications: Society and Environment*, *7*, 27-39.

Schowengerdt, R. A. (2006). *Remote sensing: models and methods for image processing*. Elsevier.

Shaw, L., Helmholz, P., Belton, D., & Addy, N. (2019). Comparison of UAV Lidar and imagery for beach monitoring. *The International Archives of Photogrammetry, Remote Sensing and Spatial Information Sciences*, *42*, 589-596.

Shivakumar, B., & Rajashekararadhya, S. (2017). Performance évaluation of spectral angle mapper and spectral correlation mapper classifiers over multiple remote sensor data. 2017 Second International Conference on Electrical, Computer and Communication Technologies (ICECCT),

Singers, N. J., Osborne, B., Lovegrove, T., Jamieson, A., Boow, J., Sawyer, J. W. D., Hill, K., Andrews, J., Hill, S., & Webb, C. (2017). *Indigenous terrestrial and wetland ecosystems of Auckland*. Auckland Council, Te Kaunihera o Tāmaki Makaurau.

Singers, N. J., & Rogers, G. M. (2014). *A classification of New Zealand's terrestrial ecosystems*. Publishing Team, Department of Conservation.

Sofonia, J., Phinn, S., Roelfsema, C., & Kendoul, F. (2019). Observing geomorphological change on an evolving coastal sand dune using SLAM-based UAV LiDAR. *Remote Sensing in Earth Systems Sciences*, *2*(4), 273-291.

Song, A., Kim, Y., & Han, Y. (2020). Uncertainty analysis for object-based change detection in very high-resolution satellite images using deep learning network. *Remote Sensing*, *12*(15), 2345.

Suo, C., McGovern, E., & Gilmer, A. (2019). Coastal dune vegetation mapping using a multispectral sensor mounted on an UAS. *Remote Sensing*, *11*(15), 1814.

Sykes, M. T., & Wilson, J. B. (1991). Vegetation of a coastal sand dune system in southern New Zealand. *Journal of Vegetation Science*, *2*(4), 531-538.

Taddia, Y., Russo, P., Lovo, S., & Pellegrinelli, A. (2020). Multispectral UAV monitoring of submerged seaweed in shallow water. *Applied Geomatics*, *12*(1), 19-34.

Thomas, Z., Turney, C., Palmer, J., Lloydd, S., Klaricich, J., & Hogg, A. (2018). Extending the observational record to provide new insights into invasive alien species in a coastal dune environment of New Zealand. *Applied Geography*, *98*, 100-109.

Tsouros, D. C., Bibi, S., & Sarigiannidis, P. G. (2019). A review on UAV-based applications for precision agriculture. *Information*, *10*(11), 349.

Tuna, C., Merciol, F., & Lefèvre, S. (2020). Spatio-Temporal Object Stability for Monitoring Evolving Areas in Satellite Image Time Series. ISPRS (Virtual Conference),

Turner, I. L., Harley, M. D., & Drummond, C. D. (2016). UAVs for coastal surveying. *Coastal Engineering*, *114*, 19-24.

Van Genderen, J., & Lock, B. (1977). Testing land-use map accuracy. *Photogrammetric Engineering and Remote Sensing*, *43*(9).

Wang, L., Li, C., Ying, Q., Cheng, X., Wang, X., Li, X., Hu, L., Liang, L., Yu, L., & Huang, H. (2012). China's urban expansion from 1990 to 2010 determined with satellite remote sensing. *Chinese Science Bulletin*, *57*(22), 2802-2812.

Xie, Y., Sha, Z., & Yu, M. (2008). Remote sensing imagery in vegetation mapping: a review. *Journal of plant ecology*, *1*(1), 9-23.

Ye, S., Pontius Jr, R. G., & Rakshit, R. (2018). A review of accuracy assessment for object-based image analysis: From per-pixel to per-polygon approaches. *ISPRS Journal of Photogrammetry and Remote Sensing*, *141*, 137-147.

Ye, S., Pontius Jr, R. G., & Rakshit, R. (2018). A review of accuracy assessment for object-based image analysis: From per-pixel to per-polygon approaches. *ISPRS Journal of Photogrammetry and Remote Sensing*, *141*, 137-147.

Zahawi, R. A., Duran, G., & Kormann, U. (2015). Sixty-seven years of land-use change in southern Costa Rica. *Plos one*, *10*(11), e0143554.

Zhang, S. L., & Chang, T. C. (2015). A study of image classification of remote sensing based on back-propagation neural network with extended delta bar delta. *Mathematical Problems in Engineering*, *2015*.

Zhang, Y., Slaughter, D. C., & Staab, E. S. (2012). Robust hyperspectral vision-based classification for multi-season weed mapping. *ISPRS Journal of Photogrammetry and Remote Sensing*, *69*, 65-73.